REPORT 1246

THE HYDRODYNAMIC CHARACTERISTICS OF MODIFIED RECTANGULAR FLAT PLATES HAVING ASPECT RATIOS OF 1.00, 0.25, AND 0.125 AND OPERATING NEAR A FREE WATER SURFACE [1]

By Kenneth L. Wadlin, John A. Ramsen, and Victor L. Vaughan, Jr.

SUMMARY

An investigation has been conducted to determine the hydrodynamic forces and moments acting on modified rectangular flat plates with aspect ratios of 1.00, 0.25, and 0.125 mounted on a single strut and operating at several depths of submersion. A simple method has been developed by modification of Falkner's vortex-lattice theory which enables the prediction of the lift characteristics in unseparated flow at large depths. This method shows good agreement with experimental data from the present tests and with aerodynamic data at all angles investigated for aspect ratios of 1.00 and 0.25 and at angles up to 16° for aspect ratio 0.125. Above 16° for aspect ratio 0.125, the predicted lift proved too high.

The experimental investigation indicated that decreasing the aspect ratio or depth of submersion caused a decrease in the lift coefficient, drag coefficient, and lift-drag ratio. The center of pressure moved aft with decreasing aspect ratio and forward with decreasing depth of submersion except for the aspect-ratio-0.125 plate at angles of attack above 8°. For these angles of attack, the center of pressure moved aft with decreasing depth of submersion.

Cavitation at the leading edge caused a gradual decrease in lift coefficient and a gradual increase in drag coefficient with little change in moment coefficient.

Two types of leading-edge separation at high angles of attack were encountered. One type, called "white water" and found only for the aspect-ratio-1.00 surface, caused a slight decrease in the lift and moment coefficients and a slight increase in the drag coefficient. The other type, called the "planing bubble" and found for all three surfaces, caused a sharp drop in the lift, drag, and moment coefficients primarily because of the loss of upper surface lift. The ventilation boundaries defining the start of the high-angle separation moved to higher speeds and higher angles as the aspect ratio was decreased.

INTRODUCTION

Interest has recently been shown in obtaining information on the force and moment characteristics of low-aspect-ratio lifting surfaces operating beneath the free water surface. In this connection, theoretical and experimental investigations have been undertaken by the National Advisory Committee for Aeronautics to determine methods of predicting the hydrodynamic characteristics of such surfaces and the effect produced on these characteristics by the proximity of the free water surface.

The problem resolves itself into two parts: first, the determination of the characteristics at depths great enough so that effects of the free surface may be neglected, and second, the determination of the changes in the characteristics which occur as the free surface is approached. The first part is essentially the same as the determination of the aerodynamic characteristics of a wing in an infinite incompressible medium. Therefore, with proper consideration of the Reynolds number, the large amount of aerodynamic theory and experimental data available for low-aspect-ratio lifting surfaces should be applicable in this case. Some of the aerodynamic theories and experimental data relating to low-aspect-ratio wings have been summarized in reference 1. In addition, the NACA has recently conducted investigations of a rectangular flat-plate wing of aspect ratio 0.25 (ref. 2) and of rectangular symmetrical wings of aspect ratios 1.0, 2.0, and 3.0 (ref. 3). The second part of the problem, which is the determination of the effects of the proximity of the free water surface, represents the difference between the hydrodynamic and aerodynamic cases. In a confined space such as a towing tank, two additional effects must be considered, namely, the effect of the finite depth (which limits the speed of wave propagation) and the effect of the rigid side walls and bottom.

The purpose of this report is to present the hydrodynamic characteristics of some low-aspect-ratio surfaces. Experimental data have been obtained in Langley tank no. 2 by using modified flat-plate surfaces with aspect ratios of 1.00, 0.25, and 0.125 mounted on a single strut and operating at various depths of submersion. A simple modification introducing nonlinearity to existing aerodynamic theory has been developed in an attempt to provide a theory which will give reasonable agreement with the lift at great depths and also be amenable to possible modification with the method of images in order to include the effects of the free water surface.

[1] Supersedes NACA TN 3079, 1954, by Kenneth L. Wadlin, John A. Ramsen, and Victor L. Vaughan, Jr., and TN 3249, 1954, by John A. Ramsen and Victor L. Vaughan, Jr.

Comparisons between the experimental data at the large depths and this modified theory as well as comparisons with other existing aerodynamic theories are presented.

A description of several flow phenomena peculiar to this investigation is also presented together with the effects of these flow changes on the hydrodynamic characteristics. The comparison with the theory mentioned previously is not valid where the flow changes occurred and therefore is not made for these regions.

SYMBOLS

A	aspect ratio
$a_0, a_1, \ldots a_n$; $b_0, b_1, \ldots b_n$; $c_0, c_1, \ldots c_n$	unknown coefficients in vorticity distribution series
b	span of lifting surface, ft
C_D	drag coefficient, $\dfrac{D}{\frac{1}{2}\rho V^2 S}$
C_L	lift coefficient, $\dfrac{L}{\frac{1}{2}\rho V^2 S}$
C_m	pitching-moment coefficient about trailing edge, $\dfrac{M}{\frac{1}{2}\rho V^2 Sc}$
c	chord of lifting surface, ft
D	drag, lb
F	position factor relating downwash control point to vortex, ft^{-1}
F_c	nondimensional position factor relating downwash control point to vortex, Fc
L	lift, lb
M	pitching moment about the trailing edge, ft-lb
S	area of lifting surface, sq ft
V	forward speed, ft/sec
w	downwash velocity, ft/sec
x, y	coordinates along the lifting surface, ft
x', y', z'	coordinates of downwash control point relative to vortex, ft
α	angle of attack, deg
Γ	circulation, ft^2/sec
γ	vorticity, ft/sec
η	dimensionless lateral coordinate, $2y/b$
θ	dimensionless longitudinal coordinate, $\cos^{-1}\dfrac{2x}{c}$
ρ	density, slugs/cu ft

The subscript 6 denotes a depth of submersion of 6 inches.

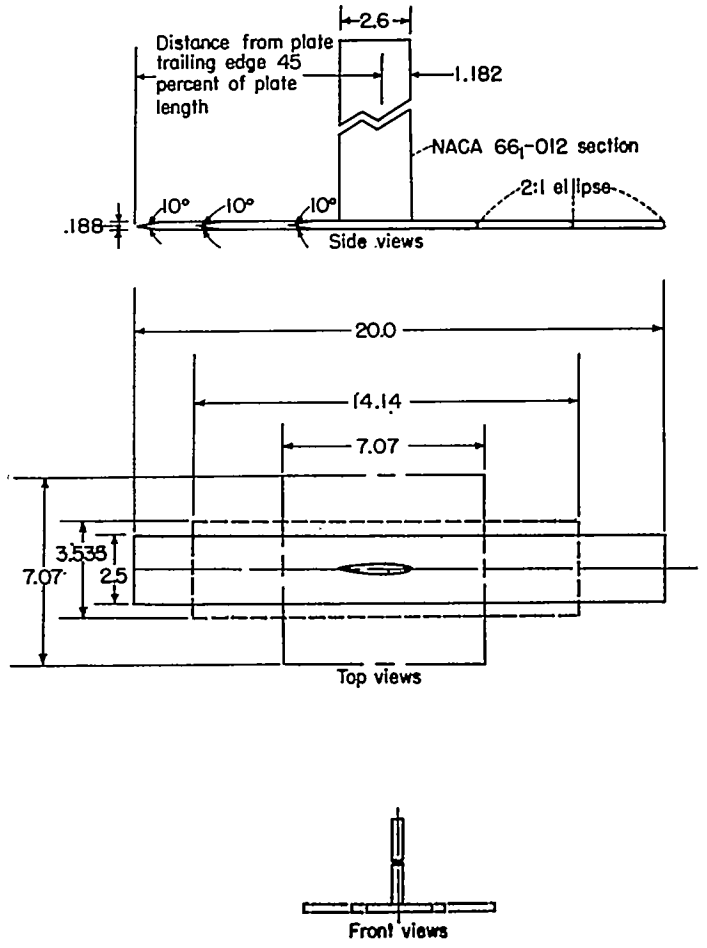

FIGURE 1.—Details of the models. (Dimensions are in inches.)

MODELS, APPARATUS, AND PROCEDURE

The models used were modified rectangular flat-plate surfaces with aspect ratios of 1.00, 0.25, and 0.125 mounted on a single strut. In order to keep the effects of the finite thickness as small as possible, the leading edges of the plates were rounded to a 2:1 ellipse and the afterportions of the plates were symmetrically beveled so that the included angle at the trailing edge was 10°. A drawing of the models is shown in figure 1.

The strut, which can also be seen in figure 1, had an NACA 66_1–012 airfoil section and was mounted so that the station 1.182 inches back of the leading edge of the strut was a distance equivalent to 45 percent of the lifting surface length forward of the trailing edge of the surface. The strut was mounted perpendicular to the plates and intersected the upper surfaces without fillets. Both the plates and the strut were made of stainless steel and were polished to a smooth finish.

Tests were made by using the Langley tank no. 2 carriage and strain-gage balances which independently measured the lift, drag, and pitching moment. The pitching moment was measured about an arbitrary point above the model and the data thus obtained were used to calculate the moments about the trailing edge at the centerline.

All tests were run with a wind screen which reduced aerodynamic tares and aerodynamic effects on flow patterns to negligible values. Before each run measurements were taken in the "at rest" condition with the model submerged and the values obtained were subtracted from the data obtained during the run; thus, the model buoyancy and strut buoyancy were not included in the data. The drag of the model included the hydrodynamic drag of the strut.

The force measurements were made at constant speeds for fixed angles of attack and depths of submersion. The depth of submersion is defined as the distance from the undisturbed water surface to the point on the model closest to the surface.

Tests were run at four depths of submersion (0.5 inch, 1.0 inch, 3.0 inches, and 6.0 inches) over a range of angle of attack from 0° to 20°. The range of speed covered at each angle of attack and depth of submersion was determined by the capacities of the balances.

The change in angle of attack due to structural deflection caused by the forces on the model was obtained during the calibration of the balances and the test data were adjusted accordingly. The depth of submersion was adjusted during each run to keep variations in this parameter to a minimum. The estimated accuracy of the measurements is as follows:

Angle of attack, deg	±0.1
Depth of submersion, in	±0.05
Speed, ft/sec	±0.2
Lift, lb	±0.25
Drag, lb	±0.10
Pitching moment, ft-lb	±0.5

The forces and moments were converted to the usual aerodynamic coefficient form by using measured values of the density. For the tests of the surfaces having aspect ratios of 1.00 and 0.25 the measured density was 1.970 slugs per cubic foot. For the aspect-ratio-0.125 tests the measured density was 1.968 slugs per cubic foot. The corresponding kinematic viscosities were 1.62×10^{-5} ft²/sec and 1.42×10^{-5} ft²/sec, respectively.

EXPERIMENTAL RESULTS

GENERAL FORCE DATA

The data obtained are presented in figures 2 to 10 as plots of lift, drag, and pitching moment about the trailing edge as functions of the angle of attack with speed as a parameter. The data are presented for all three aspect ratios at each of the four depths investigated.

Discontinuities in the drag curves at low angles of attack may be seen for all three aspect ratios at all four depths. The flow changes which cause these discontinuities were not visible during the running of the tests. At the high angles of attack and shallow depths, the discontinuities in lift, drag, and pitching-moment curves are due to the presence of leading-edge separation. These effects are discussed in the following section.

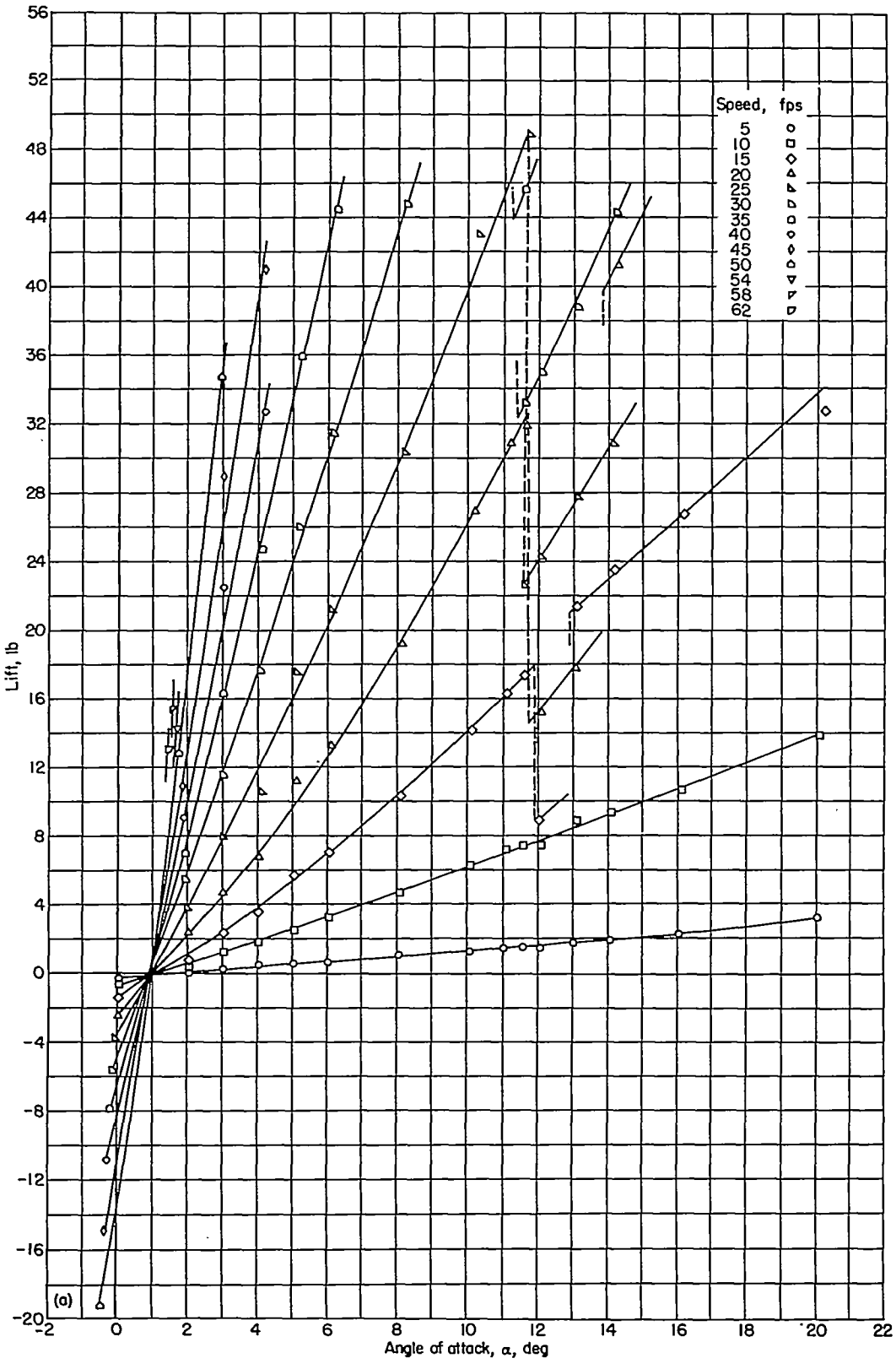

(a) Depth of submersion, 0.5 inch.

FIGURE 2.—Lift on the aspect-ratio-1.00 flat plate. (Dash lines indicate discontinuities associated with flow changes.)

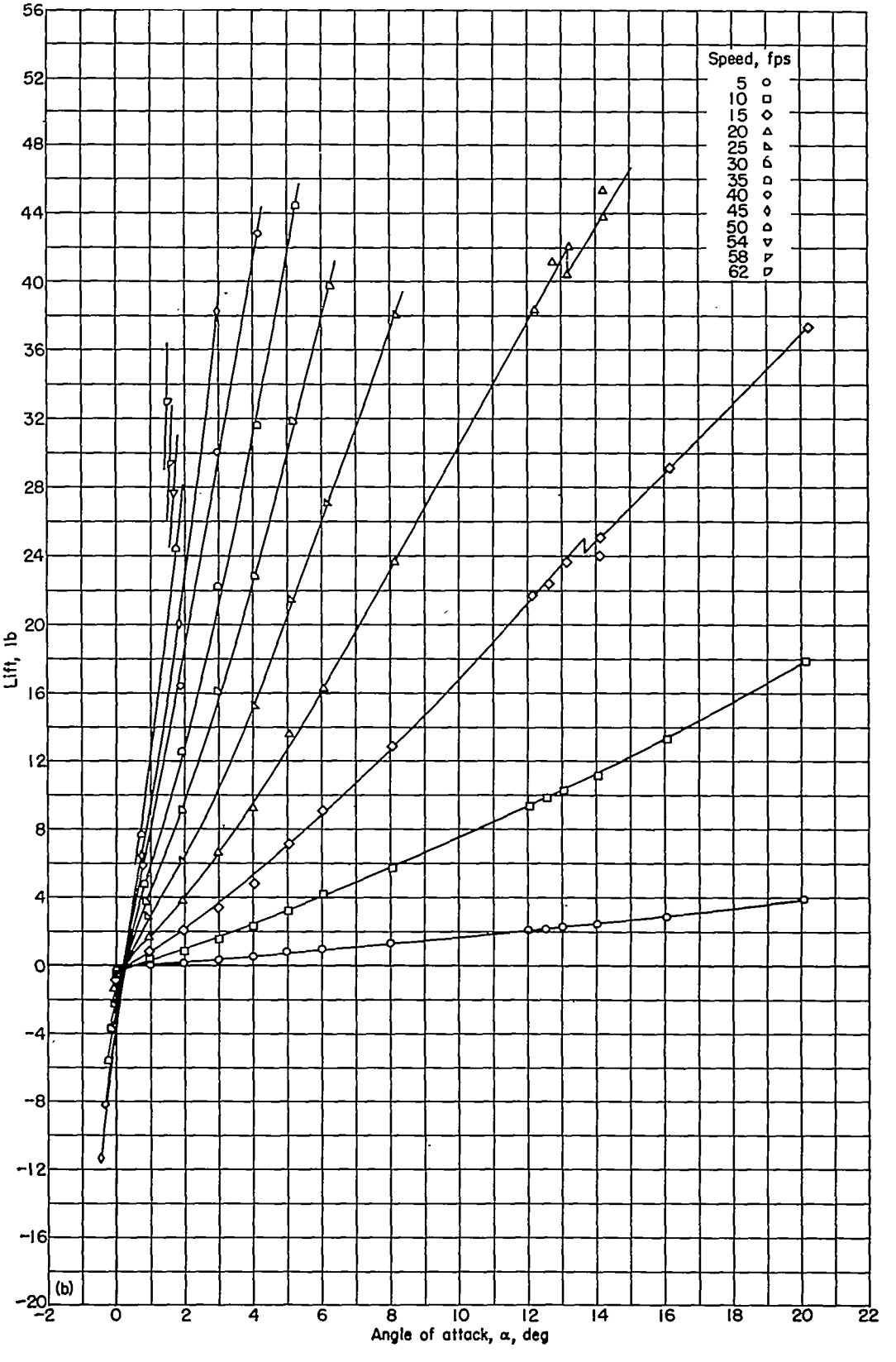

(b) Depth of submersion, 1.0 inch.

FIGURE 2.—Continued.

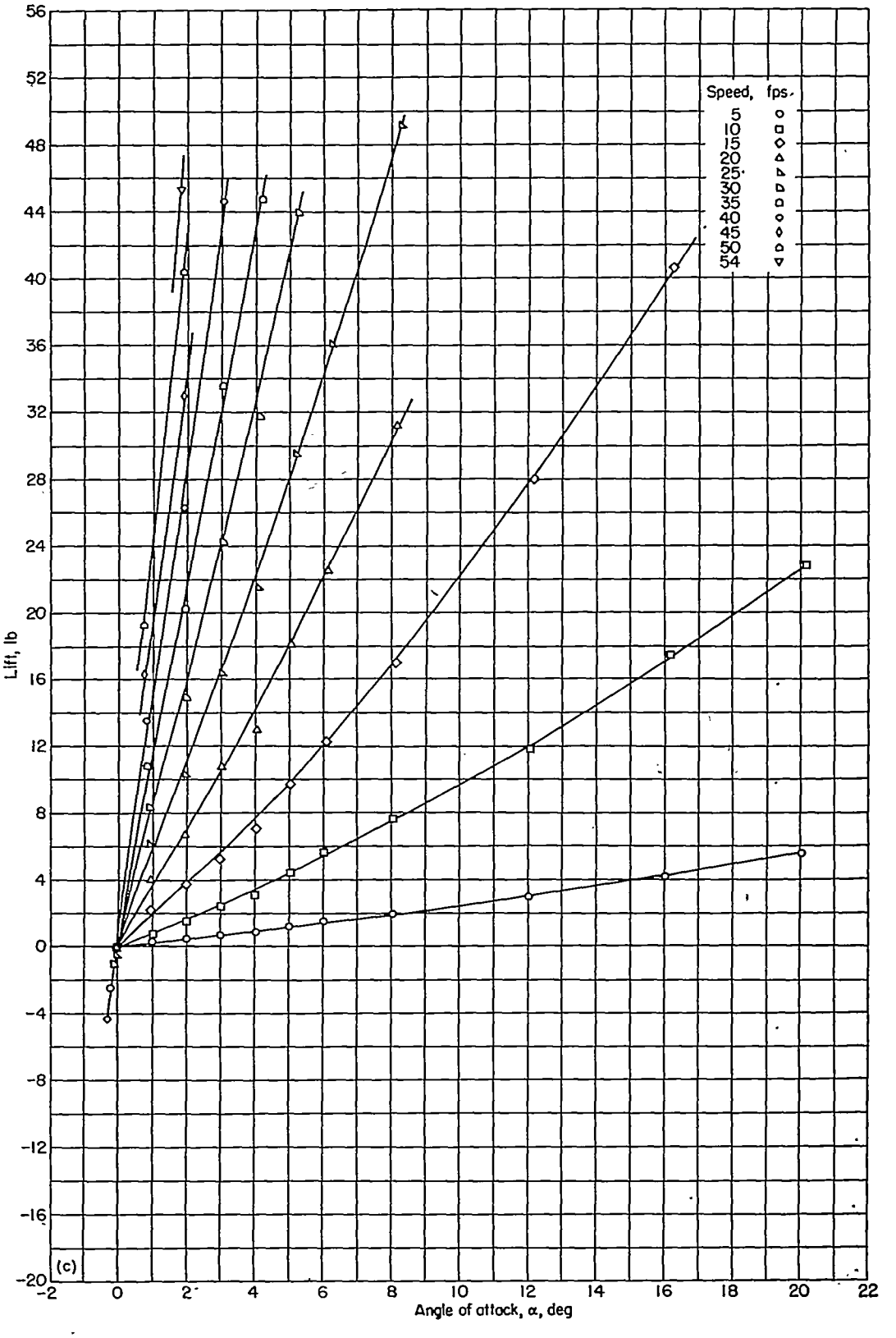

(c) Depth of submersion, 3.0 inches.

FIGURE 2.—Continued.

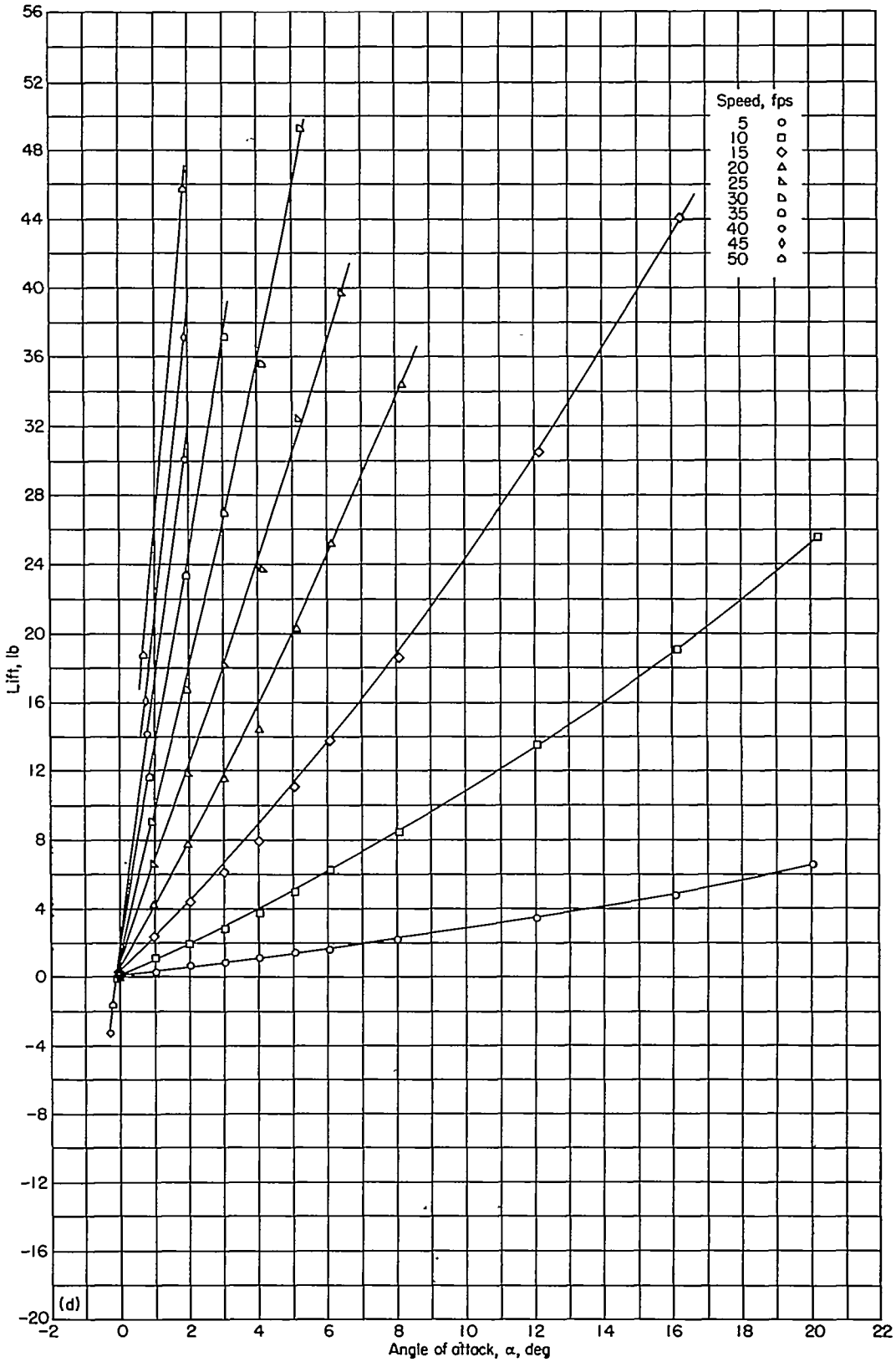

(d) Depth of submersion, 6.0 inches.

FIGURE 2.—Concluded.

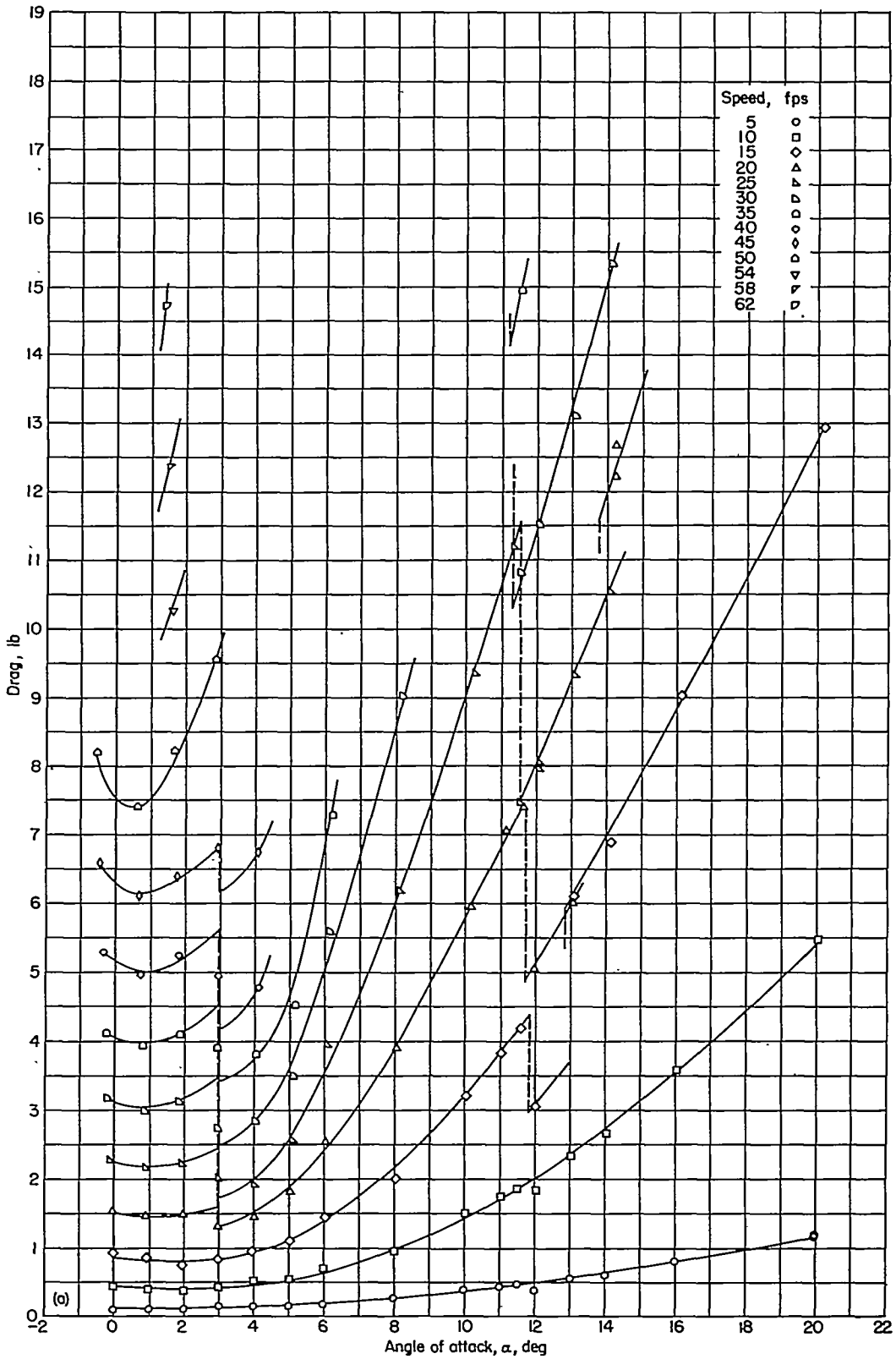

(a) Depth of submersion, 0.5 inch.

FIGURE 3.—Drag on the aspect-ratio-1.00 flat plate. (Dash lines indicate discontinuities associated with flow changes.)

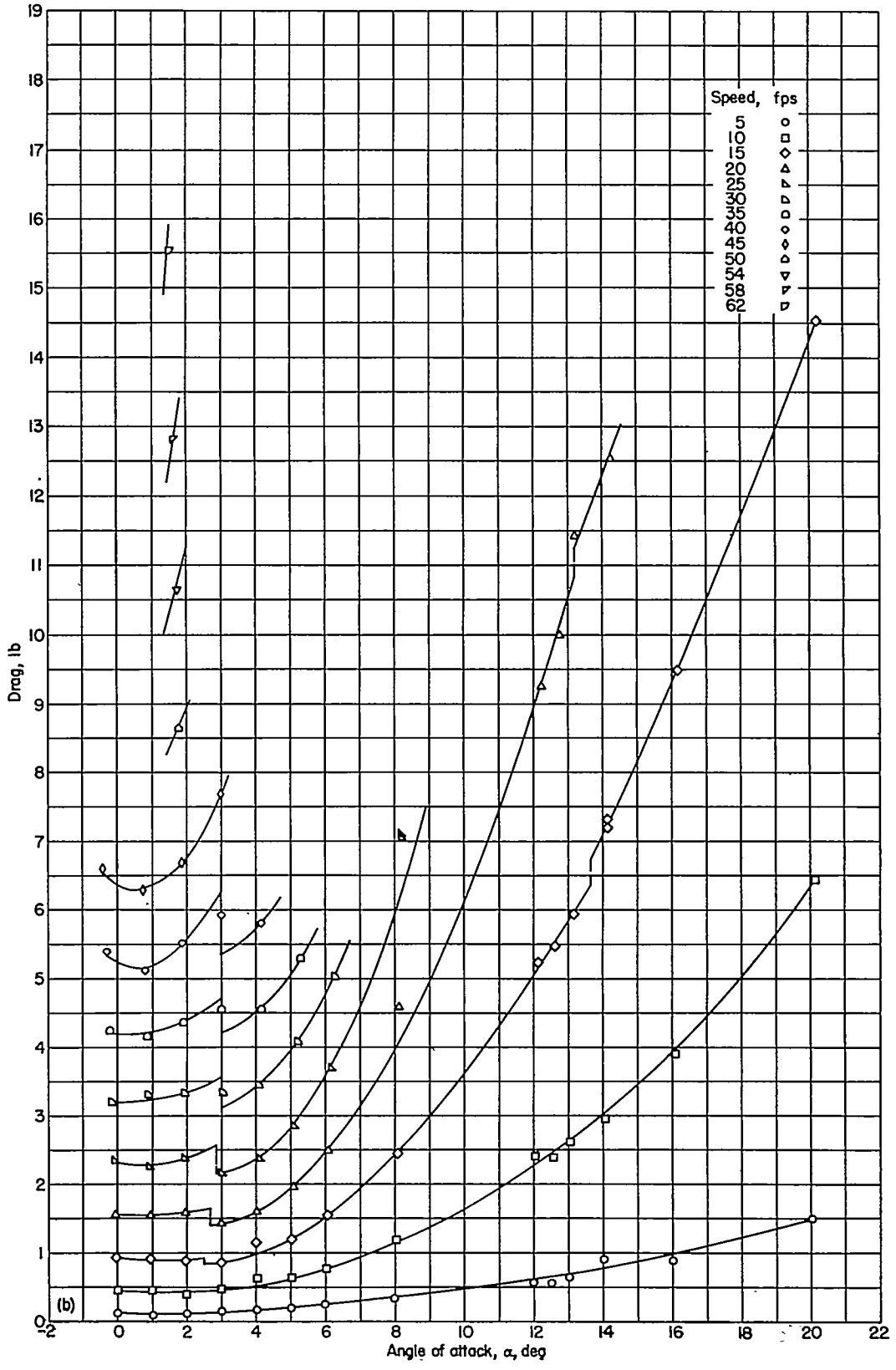

(b) Depth of submersion, 1.0 inch.

FIGURE 3.—Continued.

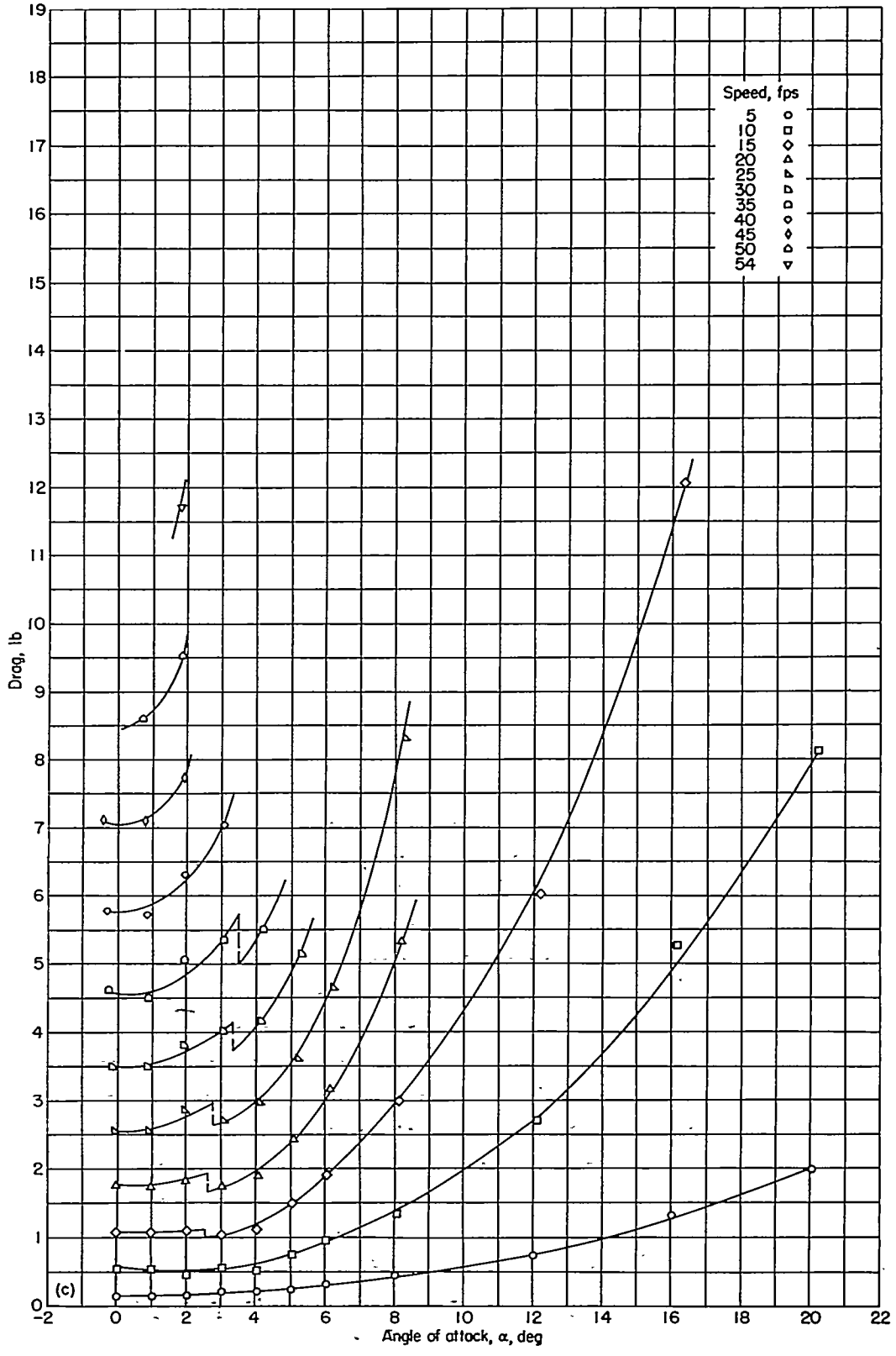

(c) Depth of submersion, 3.0 inches.

FIGURE 3.—Continued.

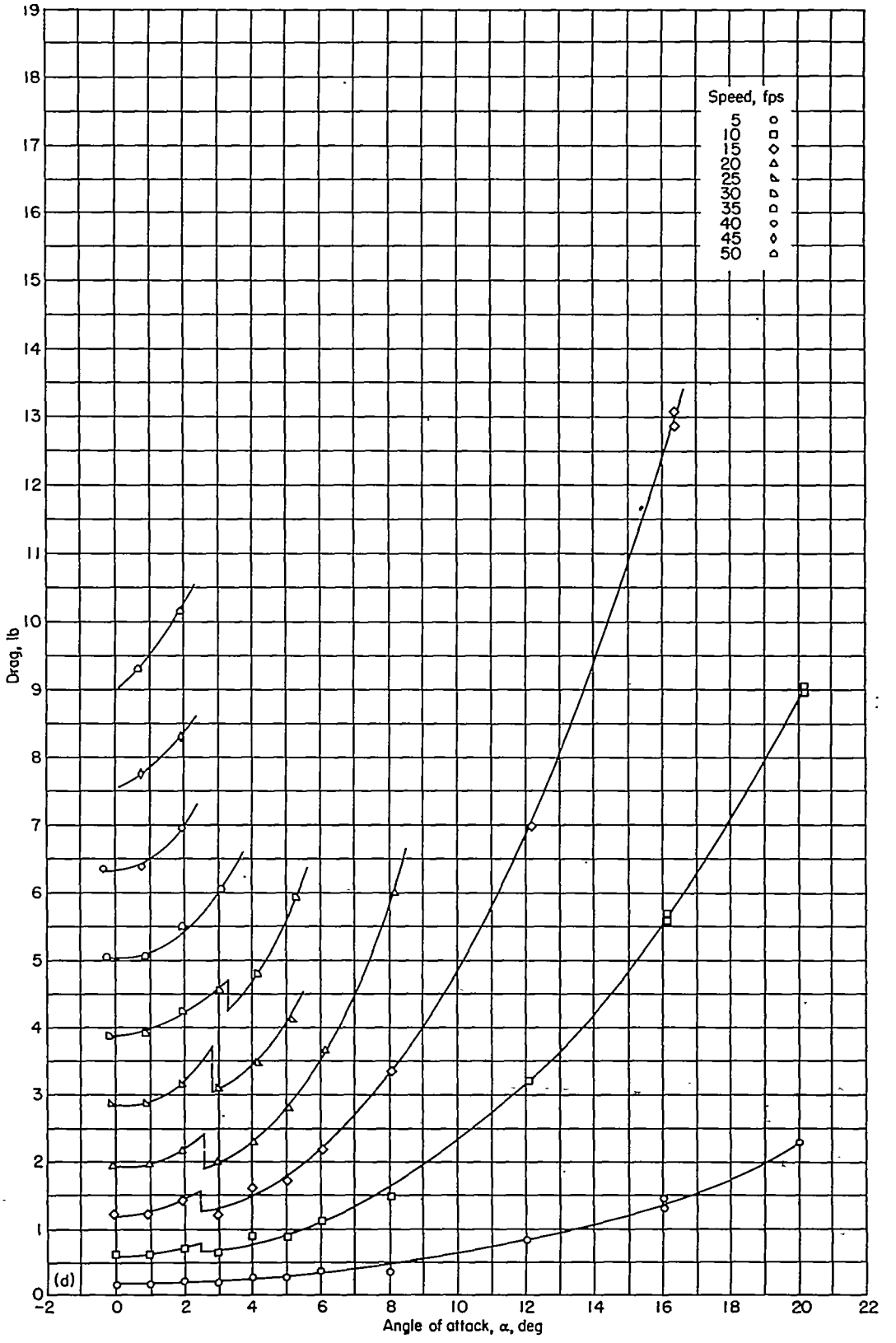

(d) Depth of submersion, 6.0 inches.

FIGURE 3.—Concluded.

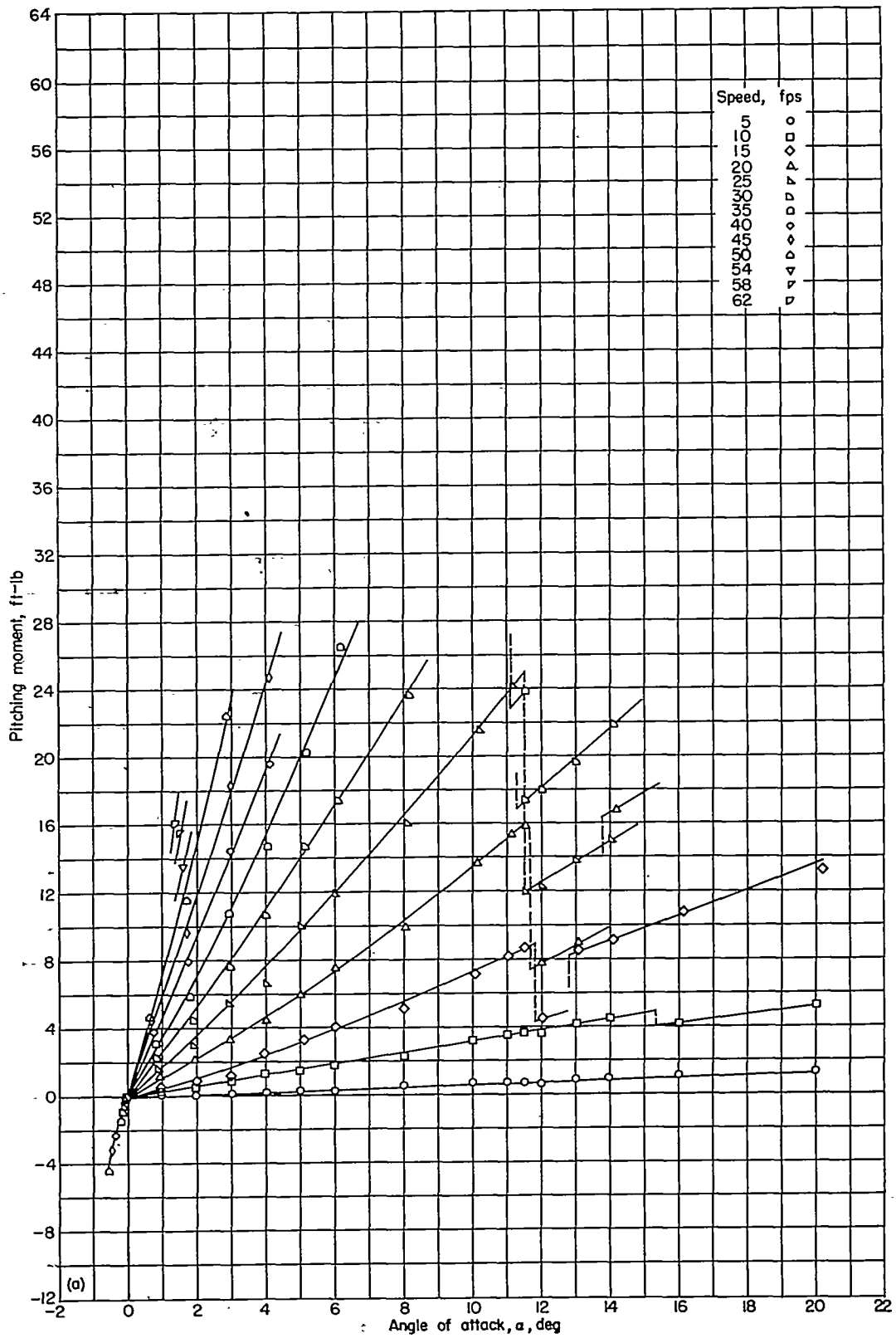

(a) Depth of submersion, 0.5 inch.

FIGURE 4.—Pitching moment on the aspect-ratio-1.00 flat plate. (Dash lines indicate discontinuities associated with flow changes.)

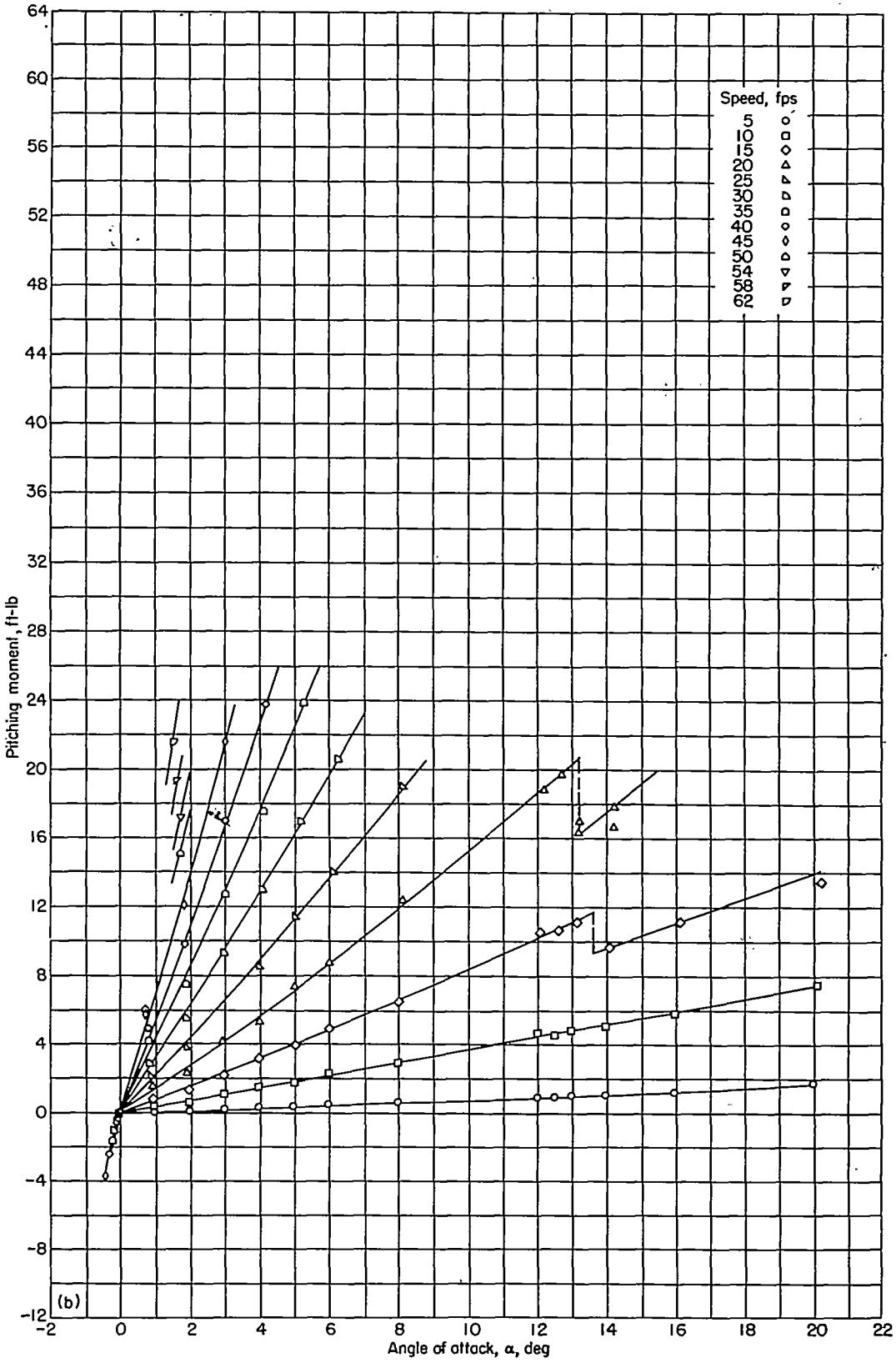

(b) Depth of submersion, 1.0 inch.

FIGURE 4.—Continued.

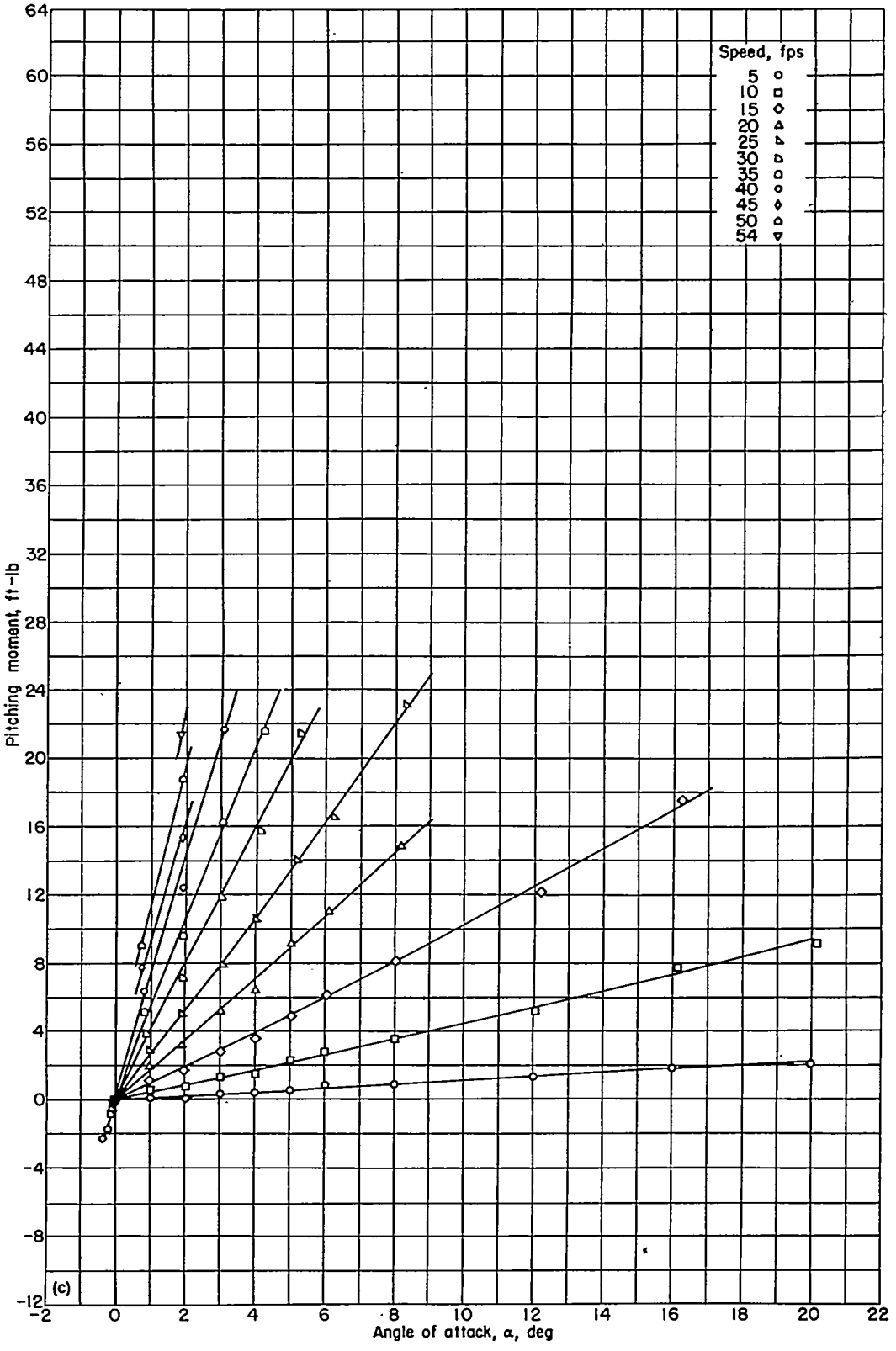

(c) Depth of submersion, 3.0 inches.

FIGURE 4.—Continued.

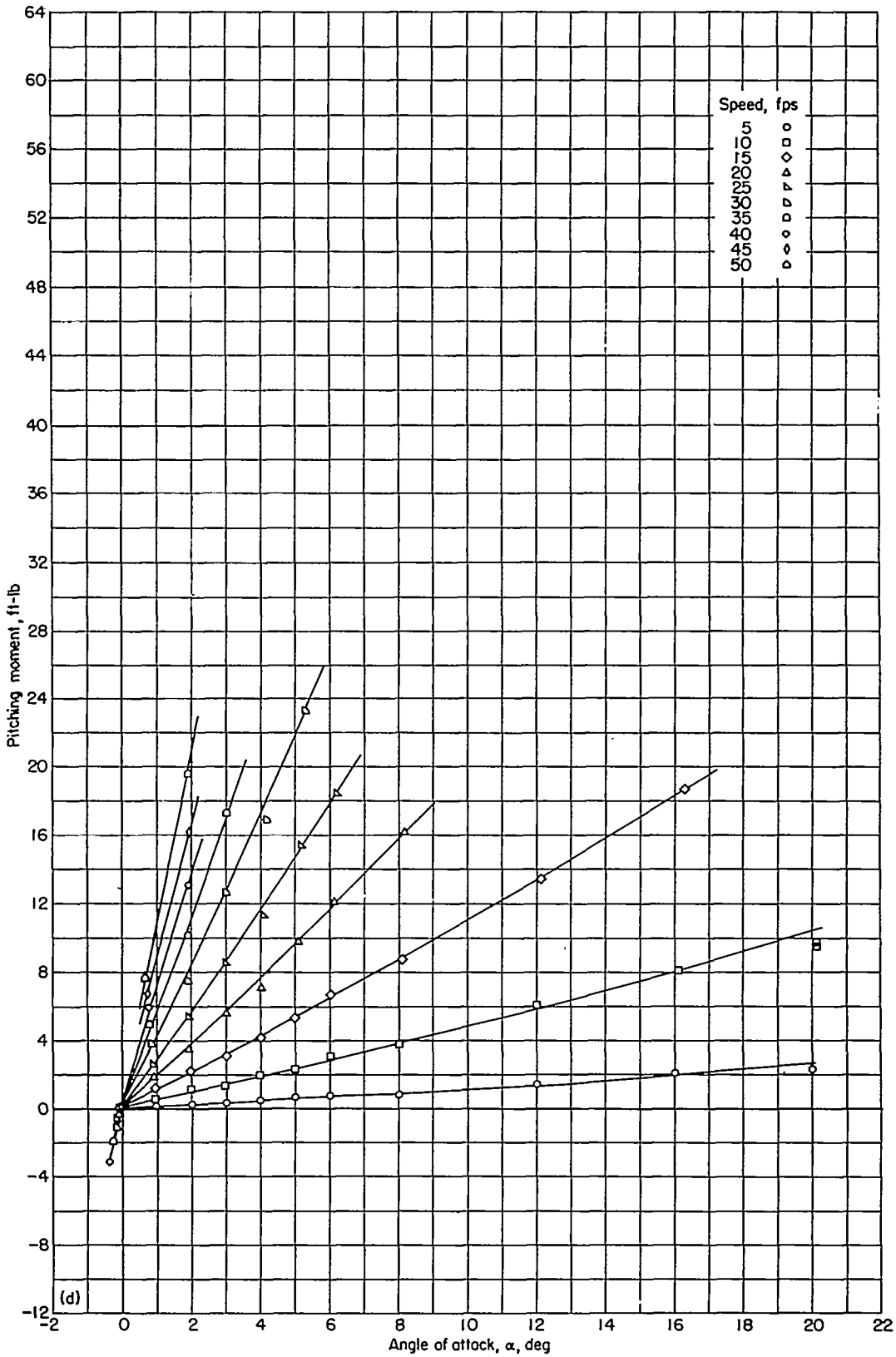

(d) Depth of submersion, 6.0 inches.

FIGURE 4.—Concluded.

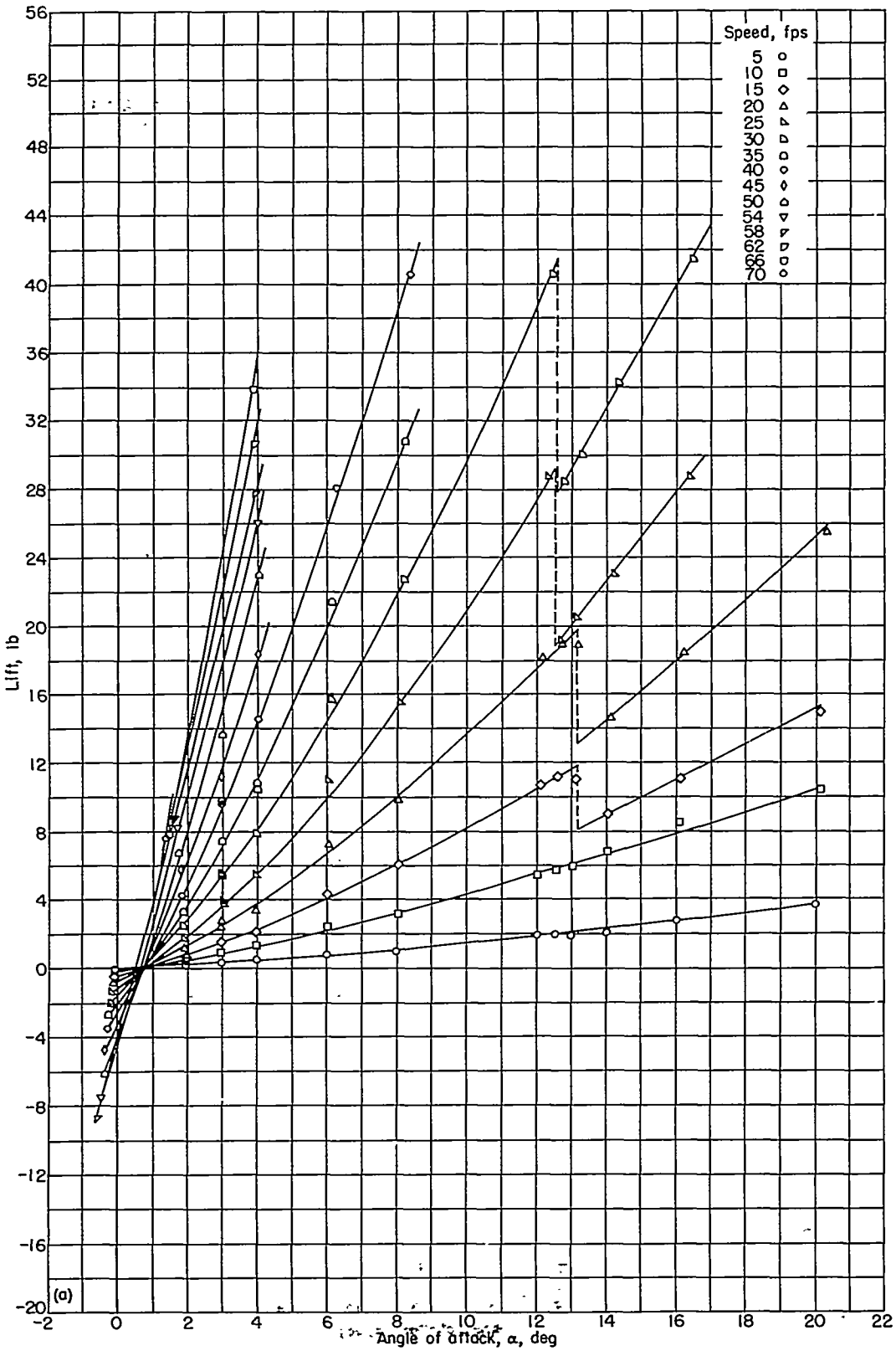

(a) Depth of submersion, 0.5 inch.

FIGURE 5.—Lift on the aspect-ratio-0.25 flat plate. (Dash lines indicate discontinuities associated with flow changes.)

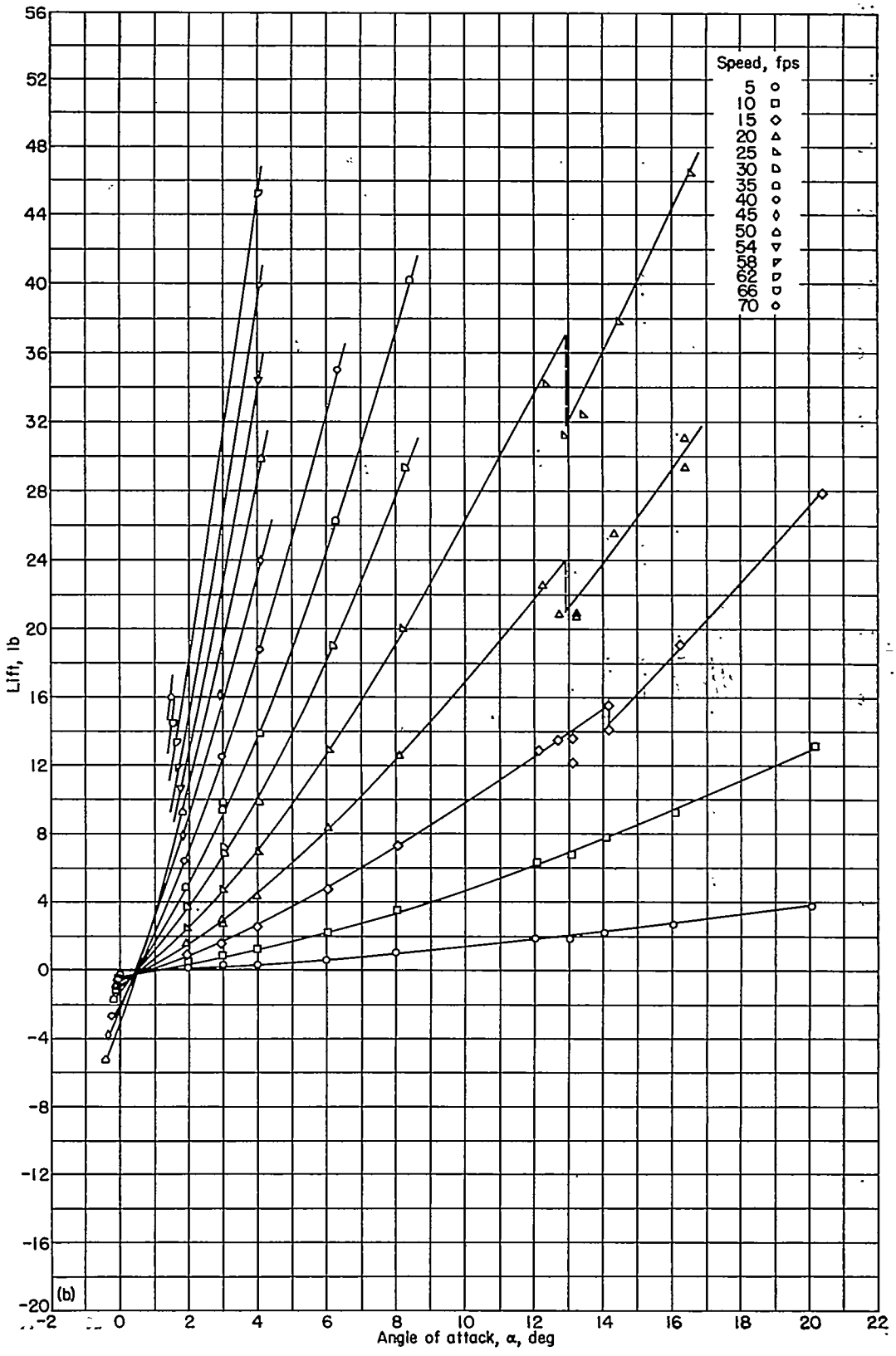

(b) Depth of submersion, 1.0 inch.

FIGURE 5.—Continued.

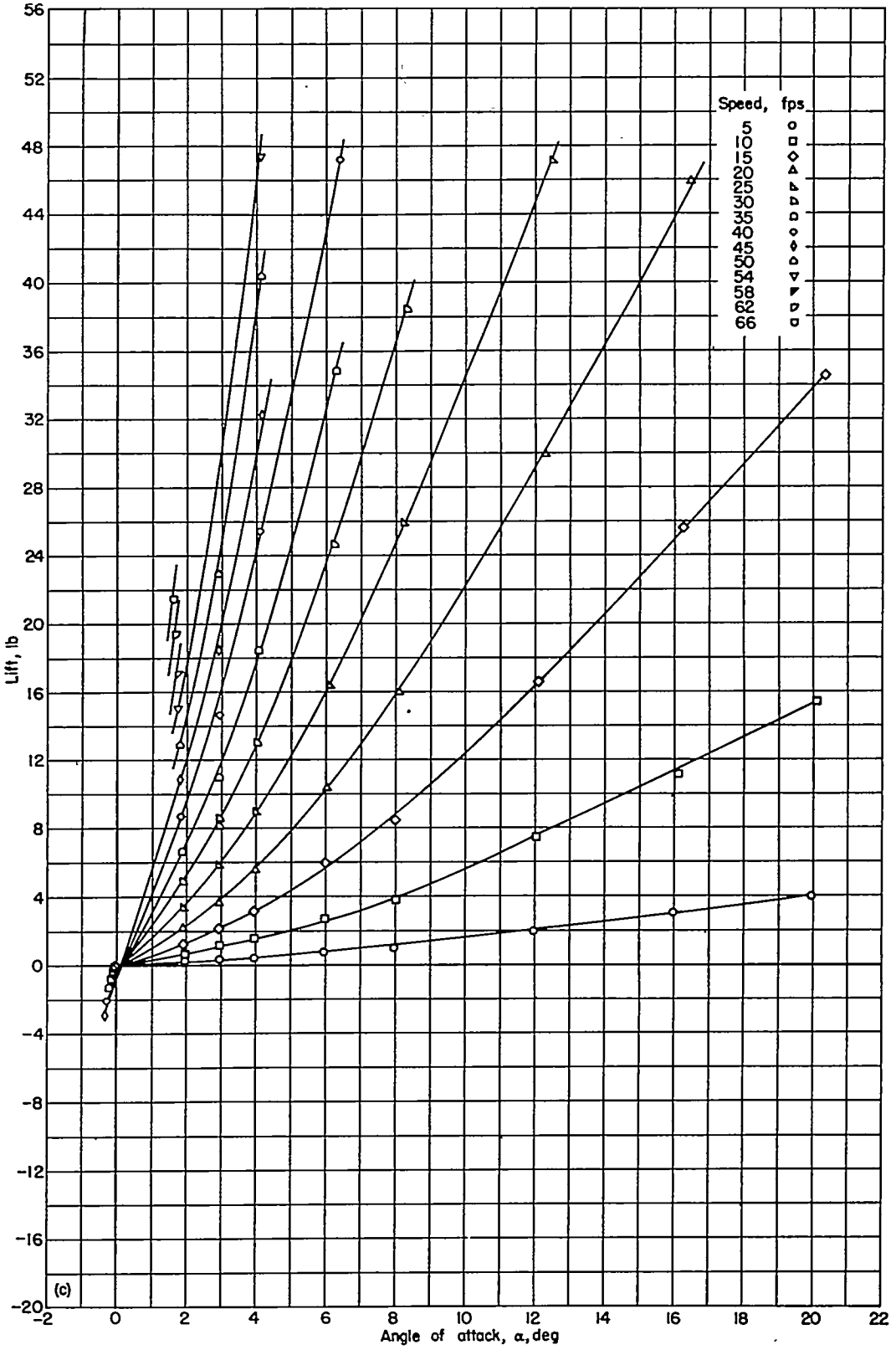

(c) Depth of submersion, 3.0 inches.

FIGURE 5.—Continued.

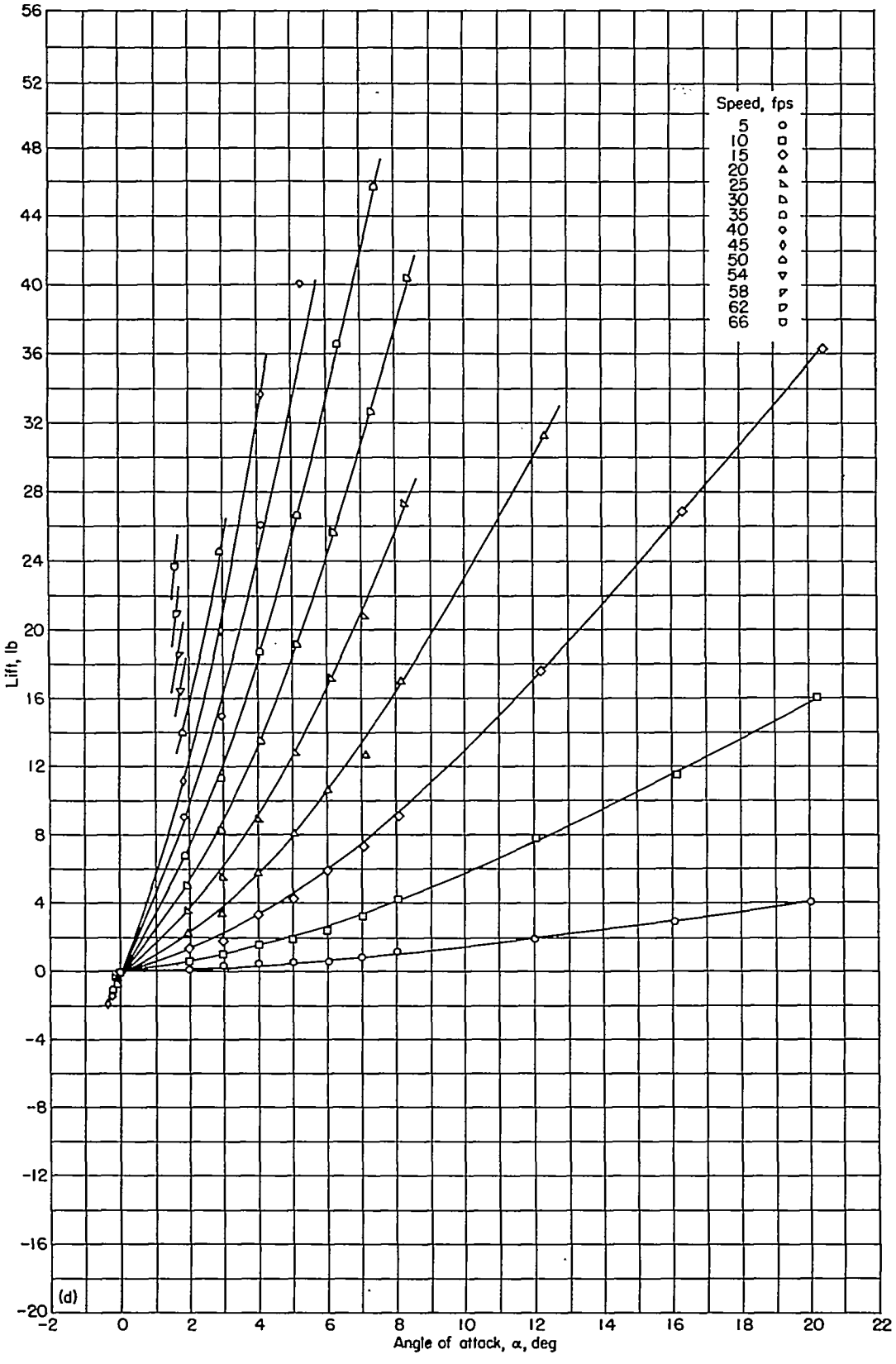

(d) Depth of submersion, 6.0 inches.

FIGURE 5.—Concluded.

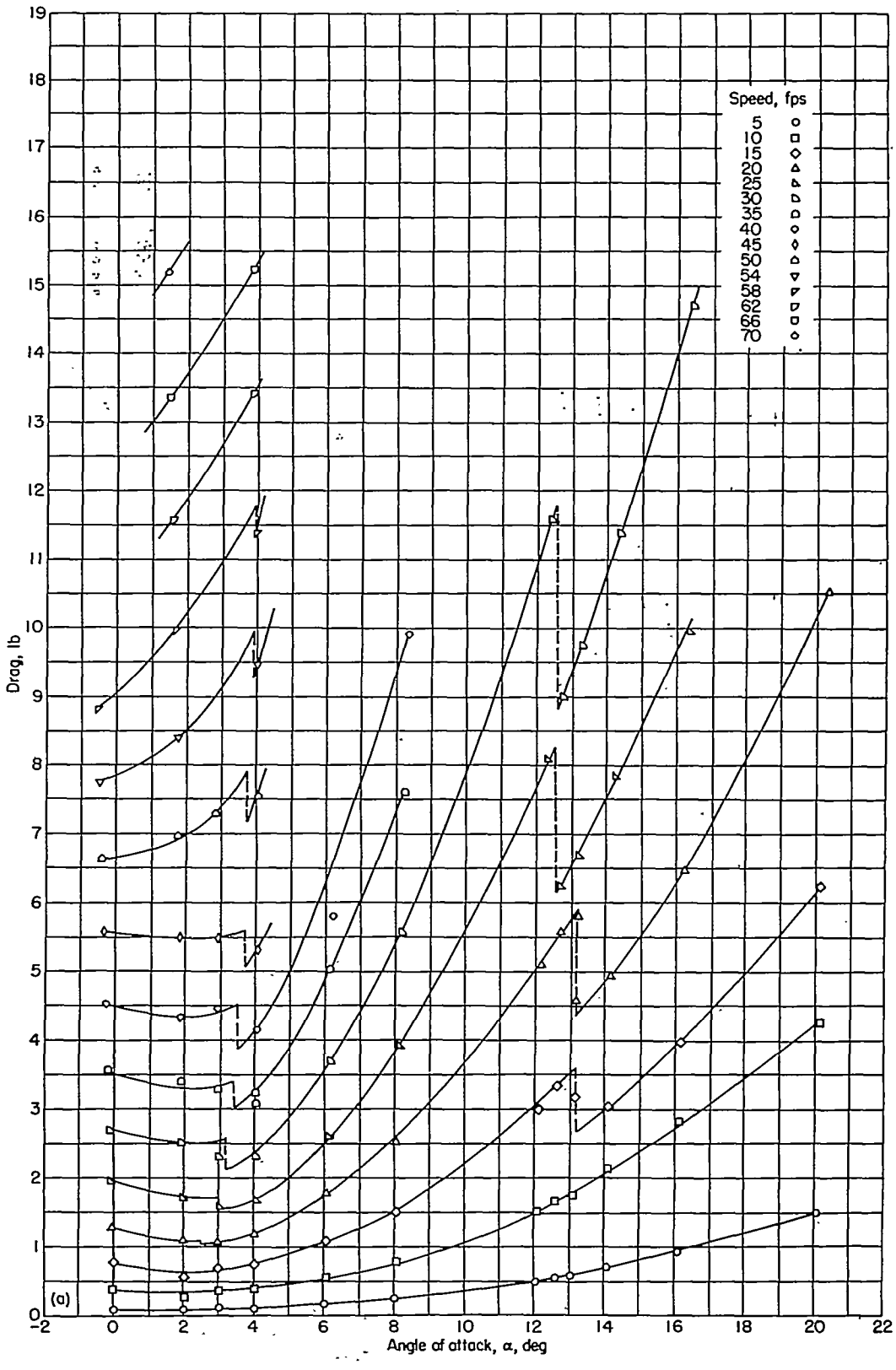

(a) Depth of submersion, 0.5 inch.

FIGURE 6.—Drag on the aspect-ratio-0.25 flat plate. (Dash lines indicate discontinuities associated with flow changes.)

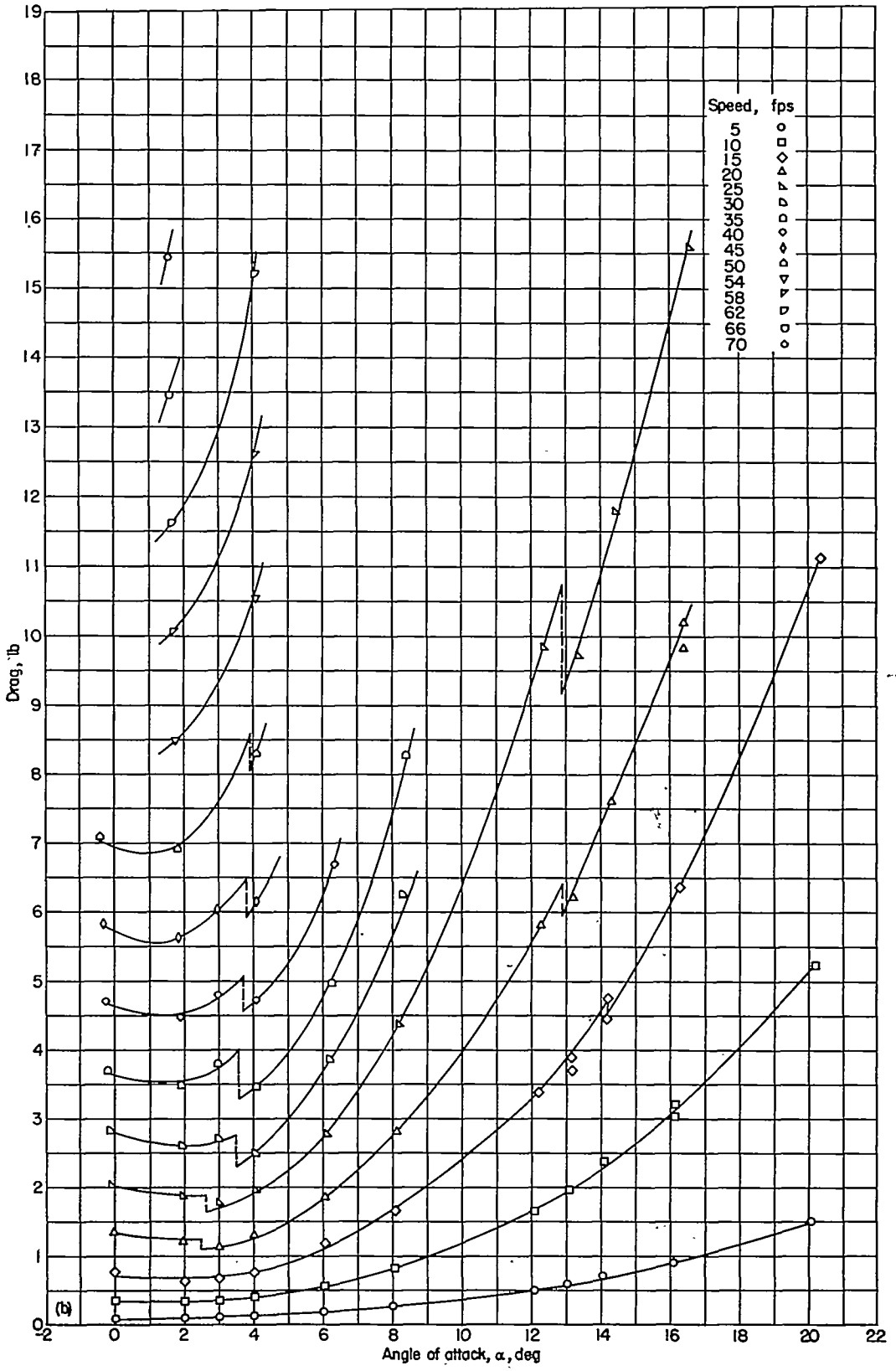

(b) Depth of submersion, 1.0 inch.

FIGURE 6.—Continued.

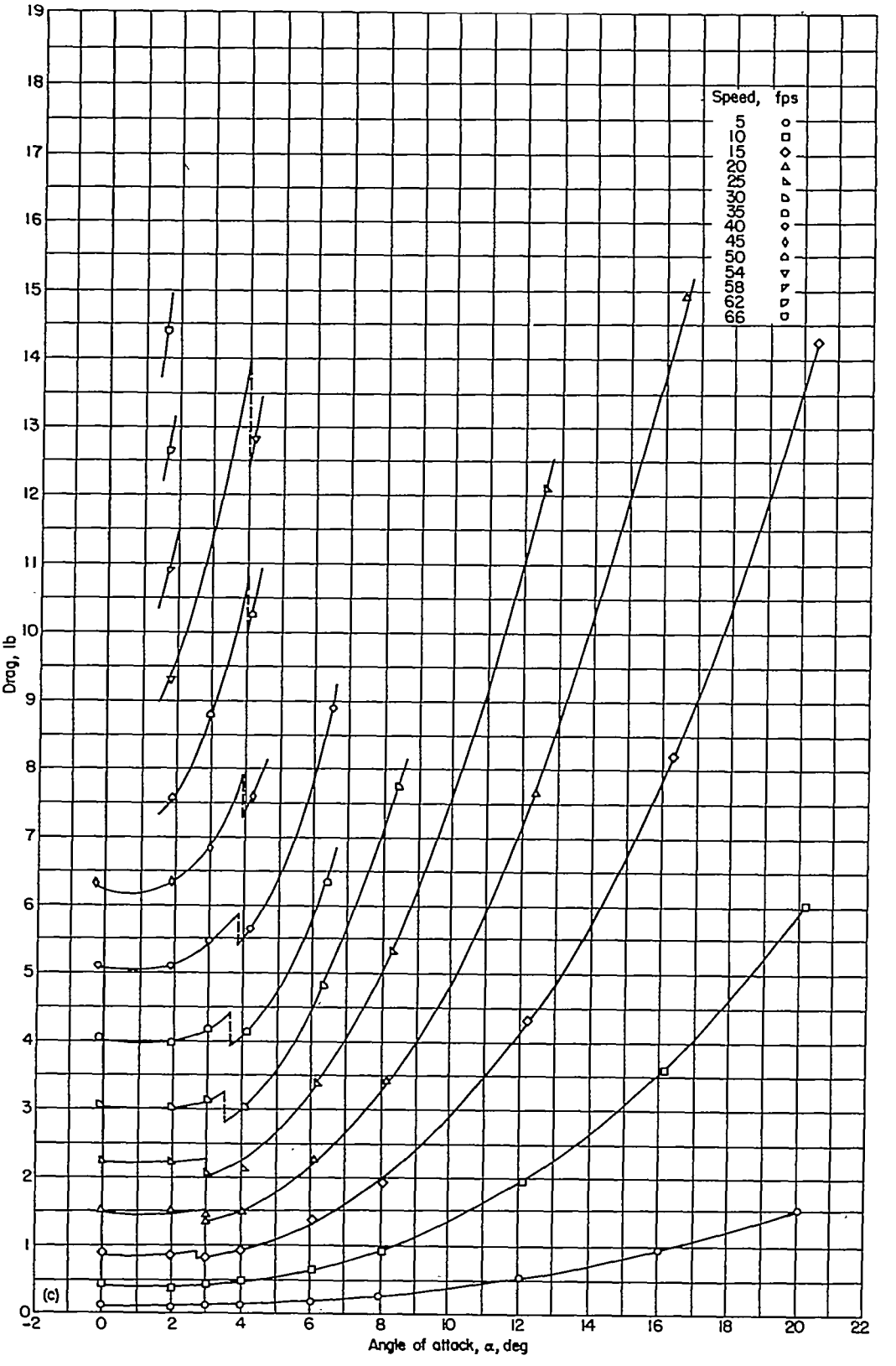

(c) Depth of submersion, 3.0 inches.

FIGURE 6.—Continued.

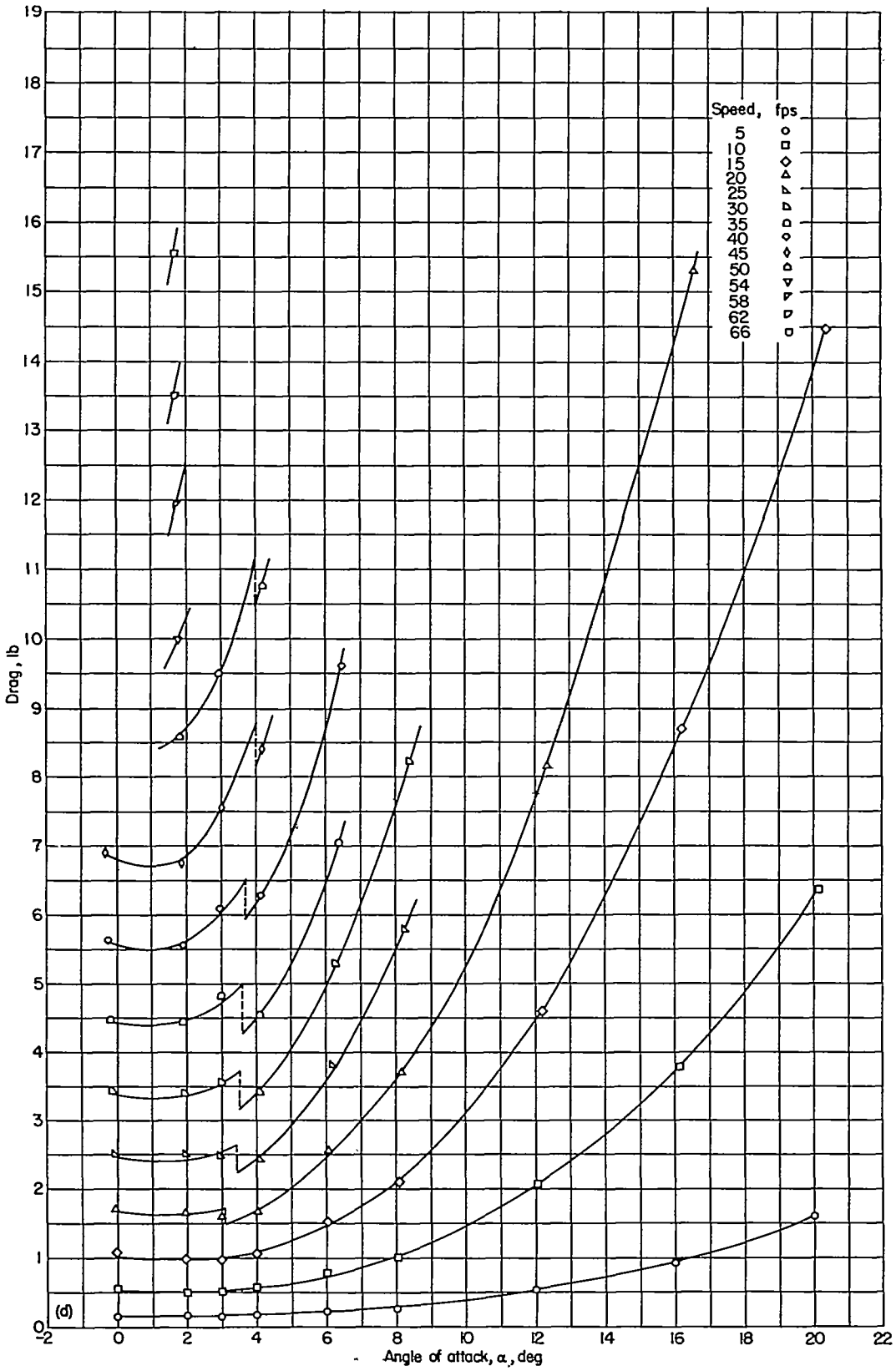

(d) Depth of submersion, 6.0 inches.

FIGURE 6.—Concluded.

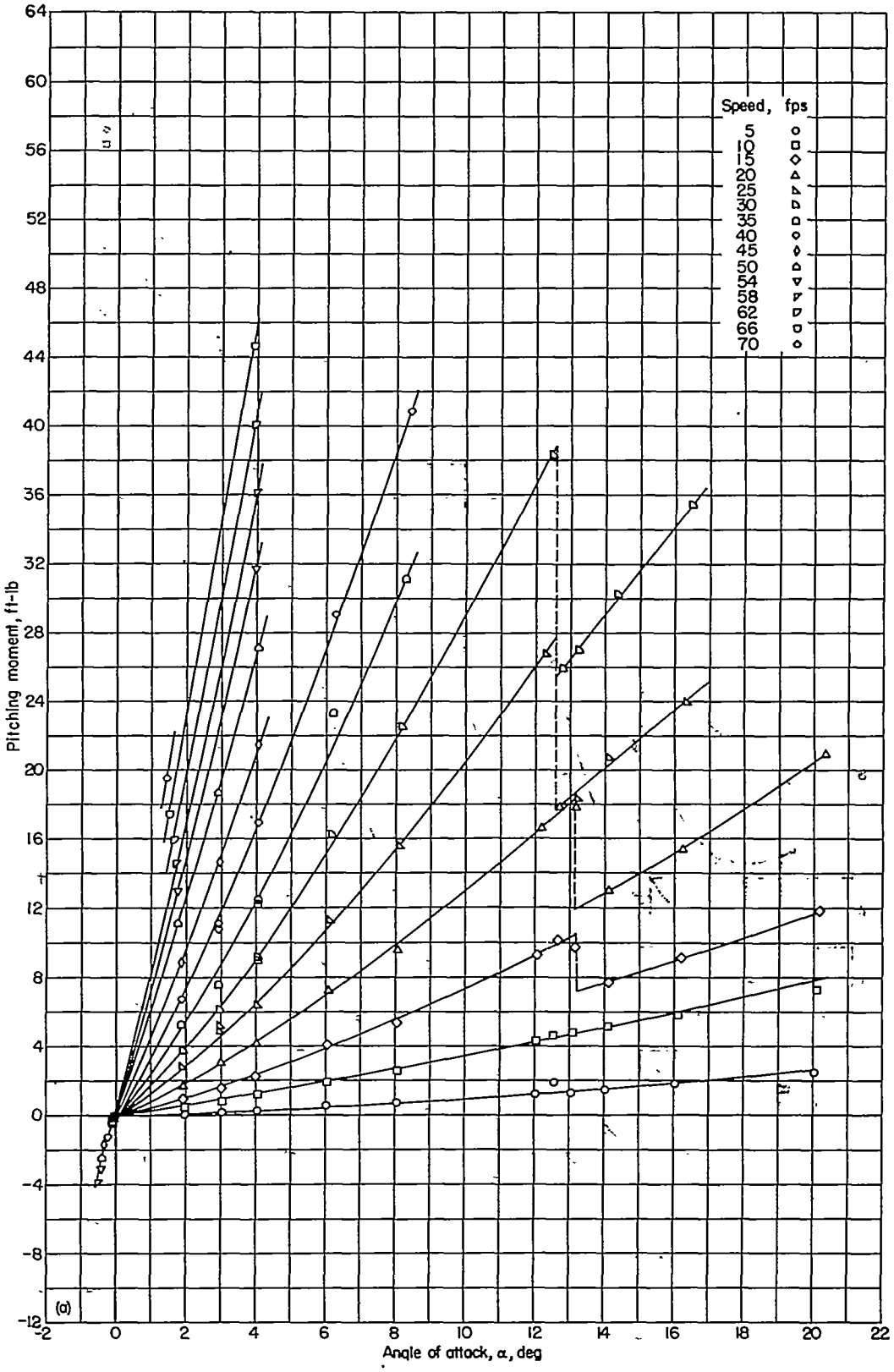

(a) Depth of submersion, 0.5 inch.

FIGURE 7.—Pitching moment on the aspect-ratio-0.25 flat plate. (Dash lines indicate discontinuities associated with flow changes.)

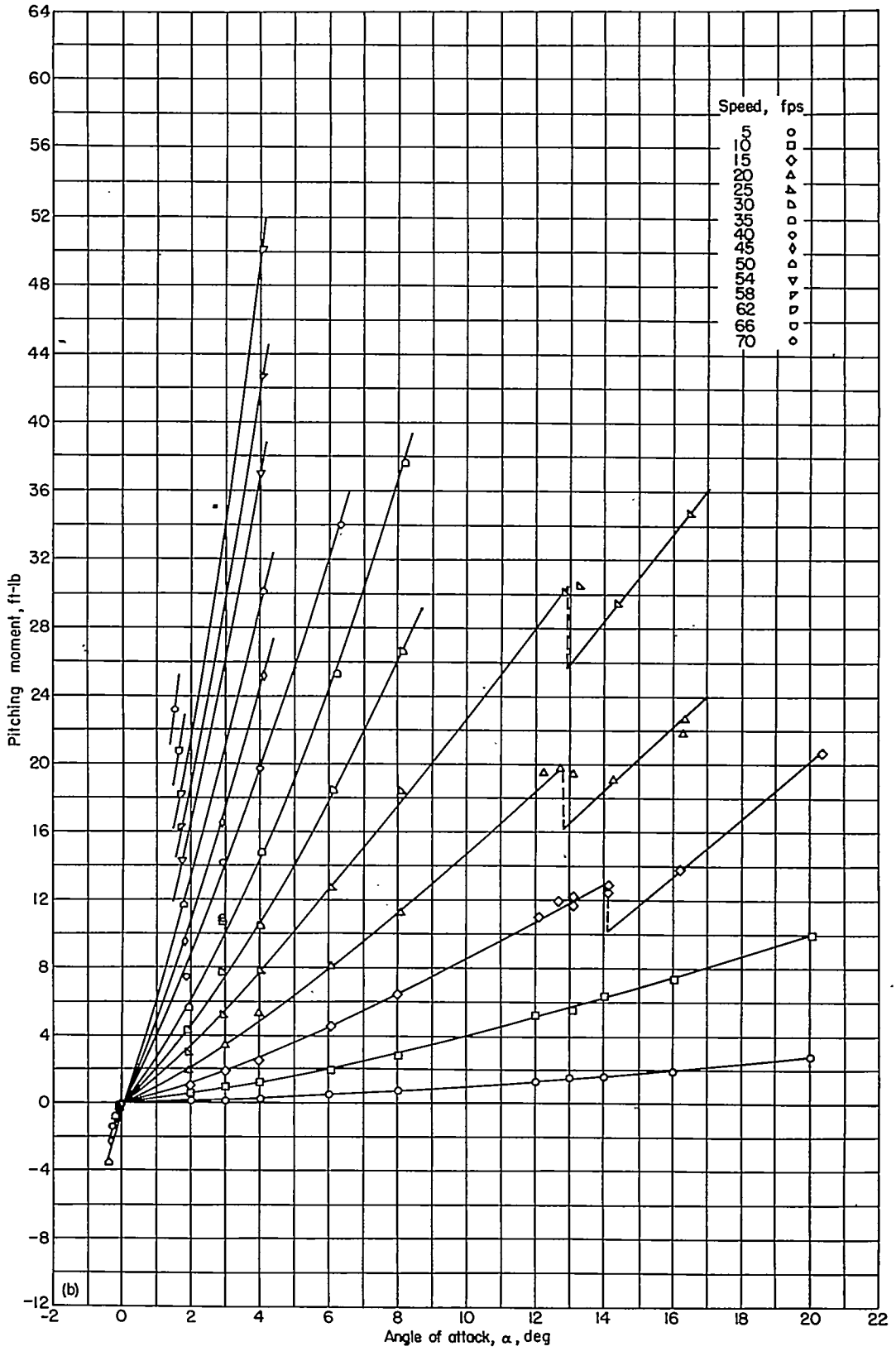

(b) Depth of submersion, 1.0 inch.

FIGURE 7.—Continued.

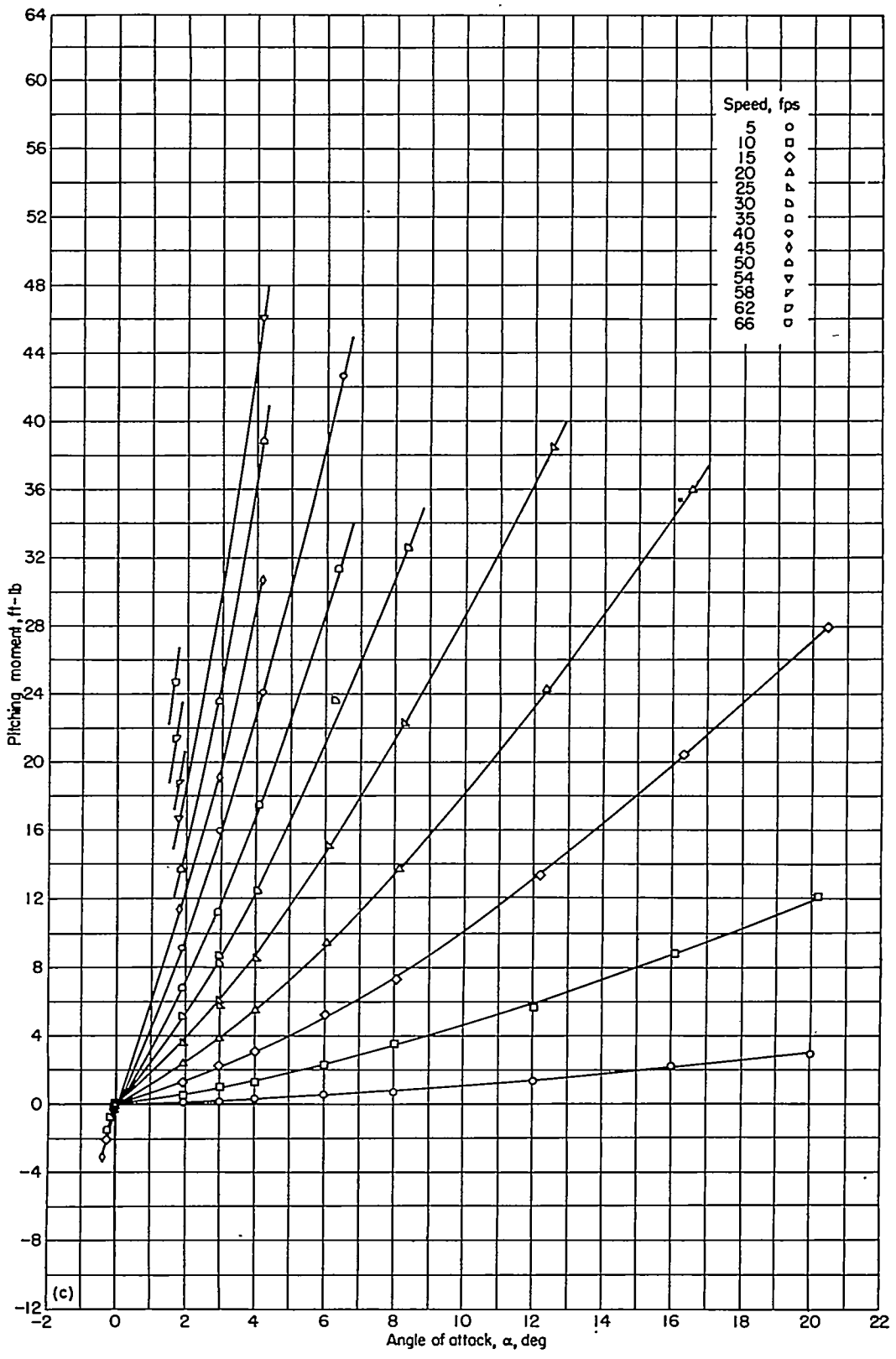

(c) Depth of submersion, 3.0 inches.

FIGURE 7.—Continued.

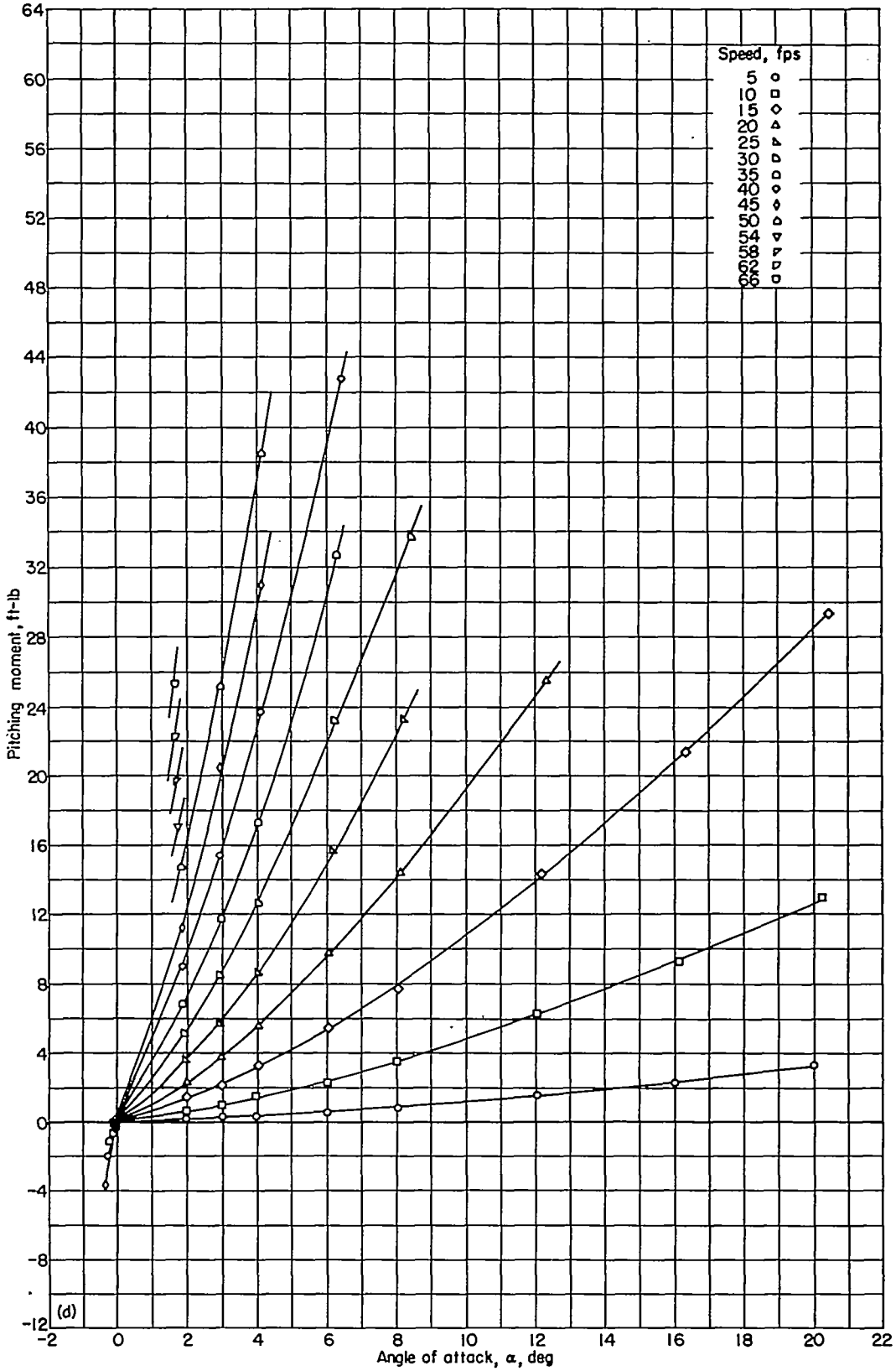

(d) Depth of submersion, 6.0 inches.

FIGURE 7.—Concluded.

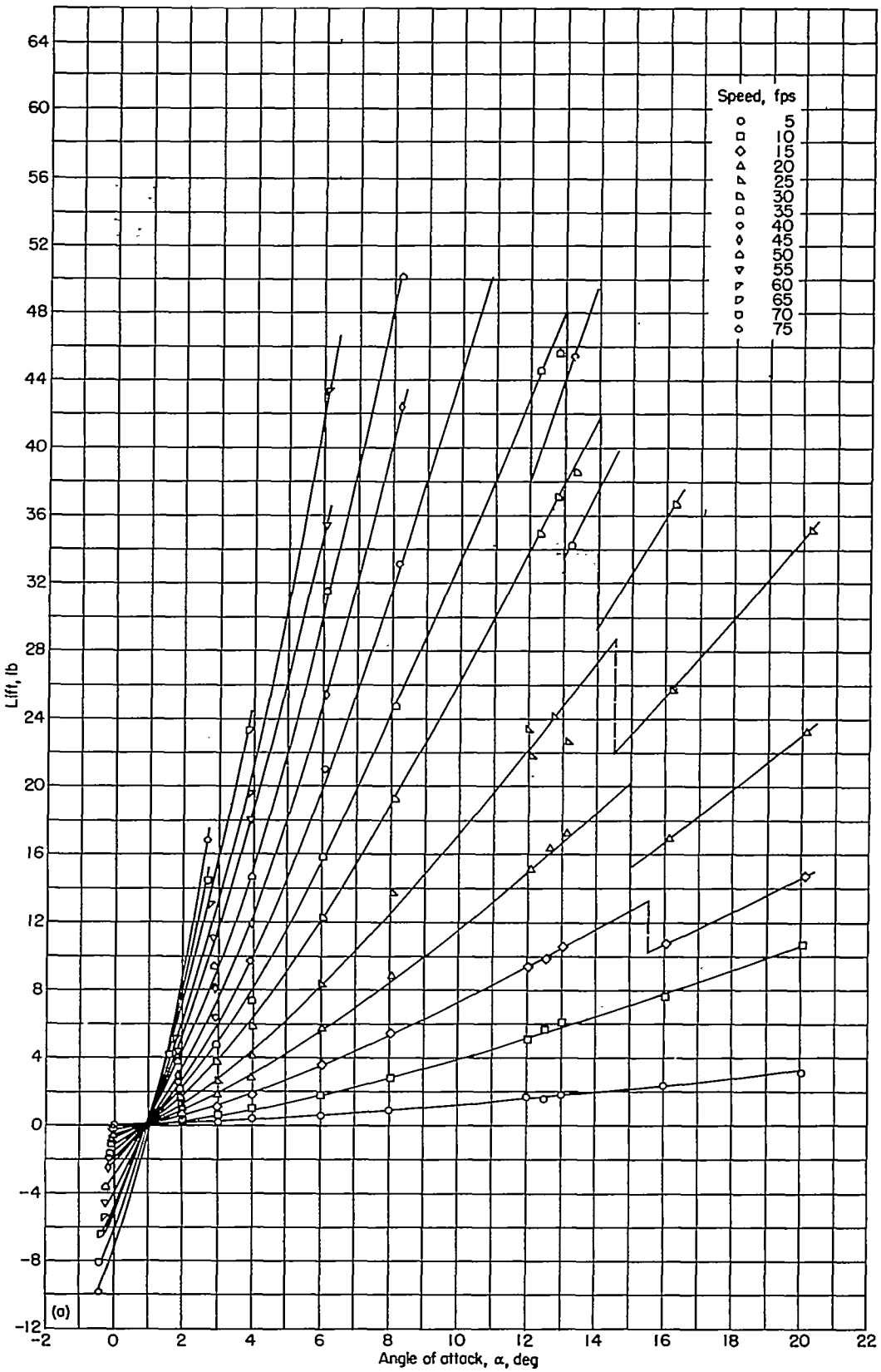

(a) Depth of submersion, 0.5 inch.

FIGURE 8.—Lift on the aspect-ratio-0.125 flat plate. (Dash lines indicate discontinuities associated with flow changes.)

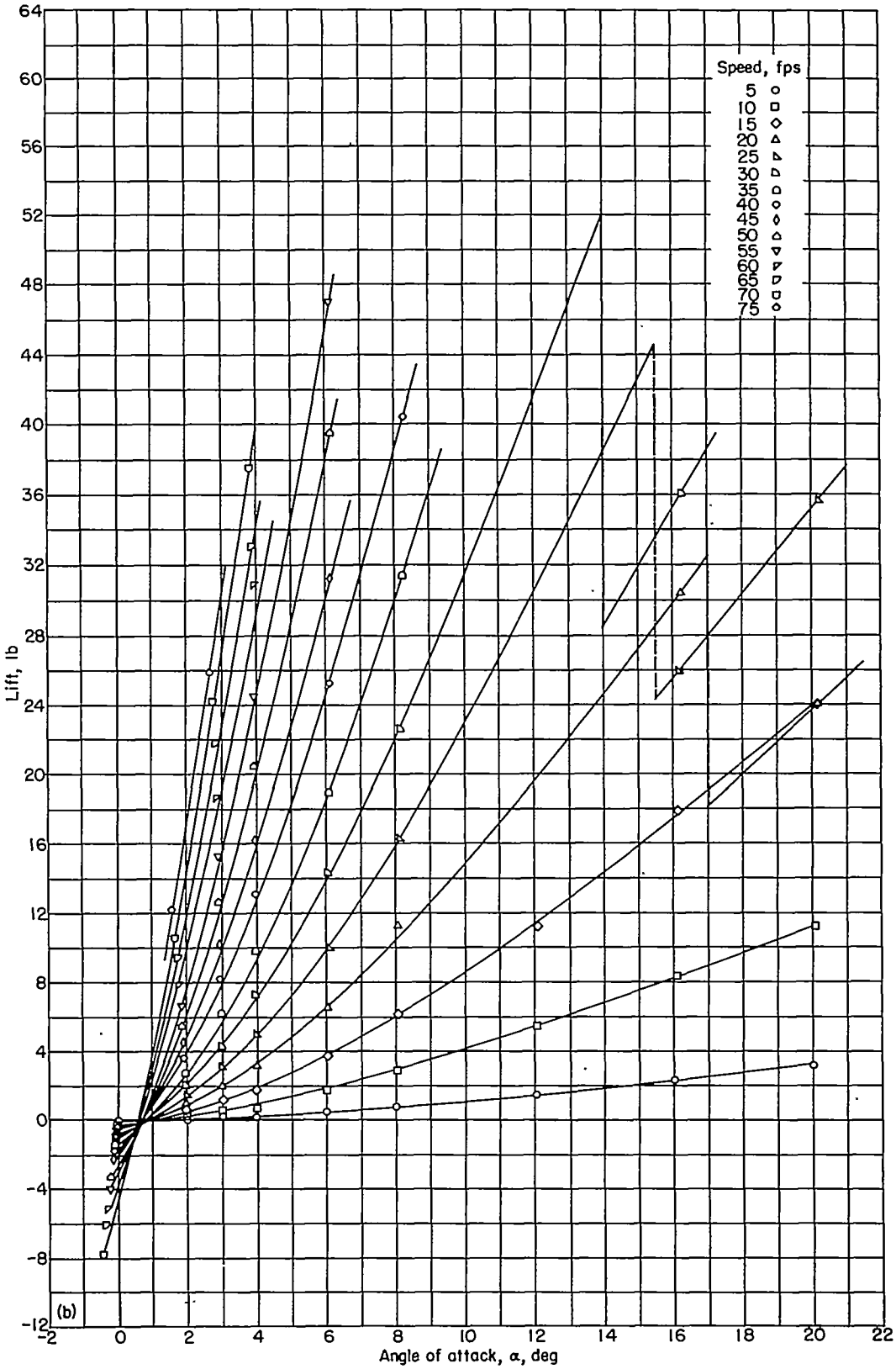

(b) Depth of submersion, 1.0 inch.

FIGURE 8.—Continued.

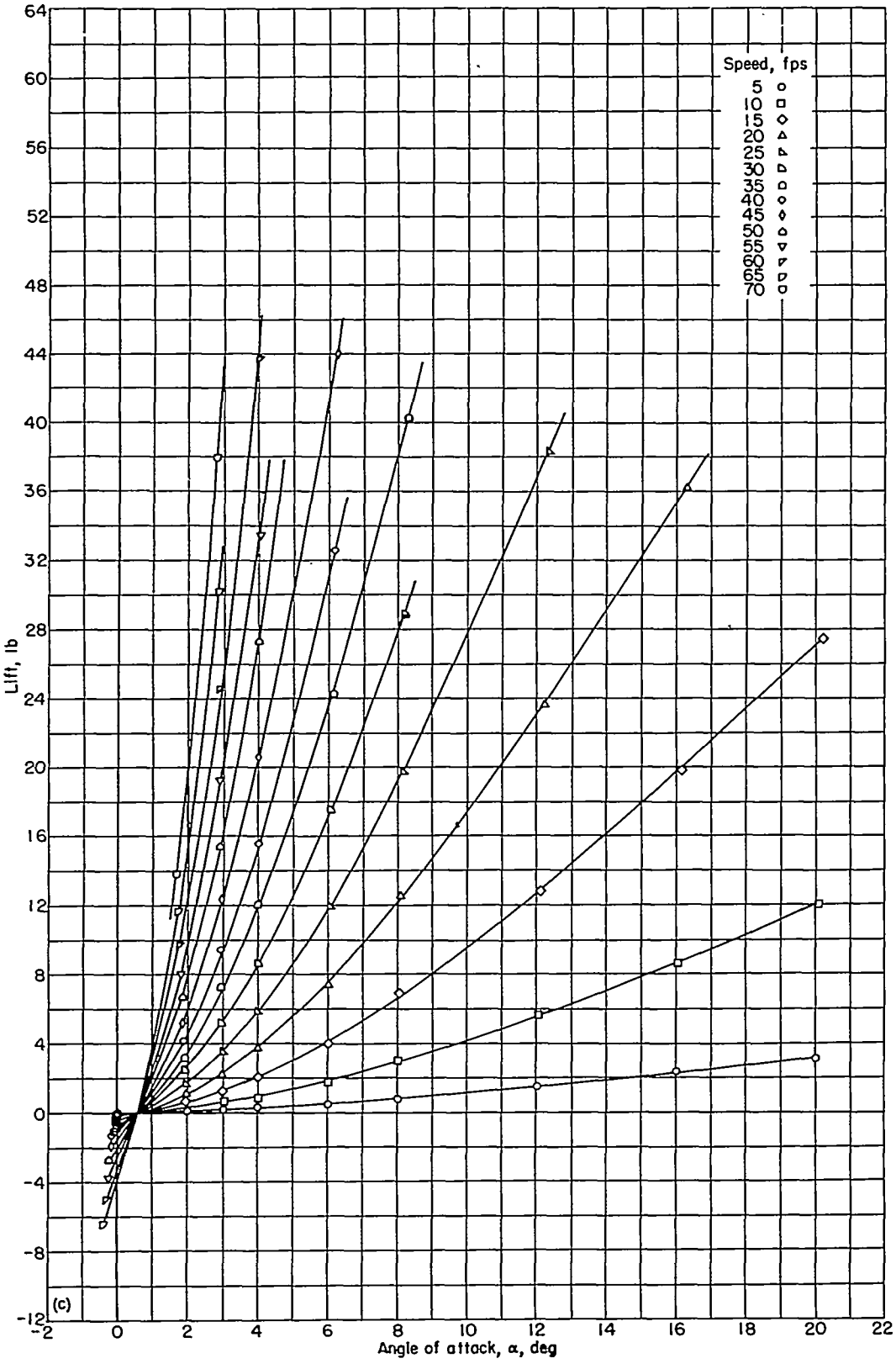

(c) Depth of submersion, 3.0 inches.

FIGURE 8.—Continued.

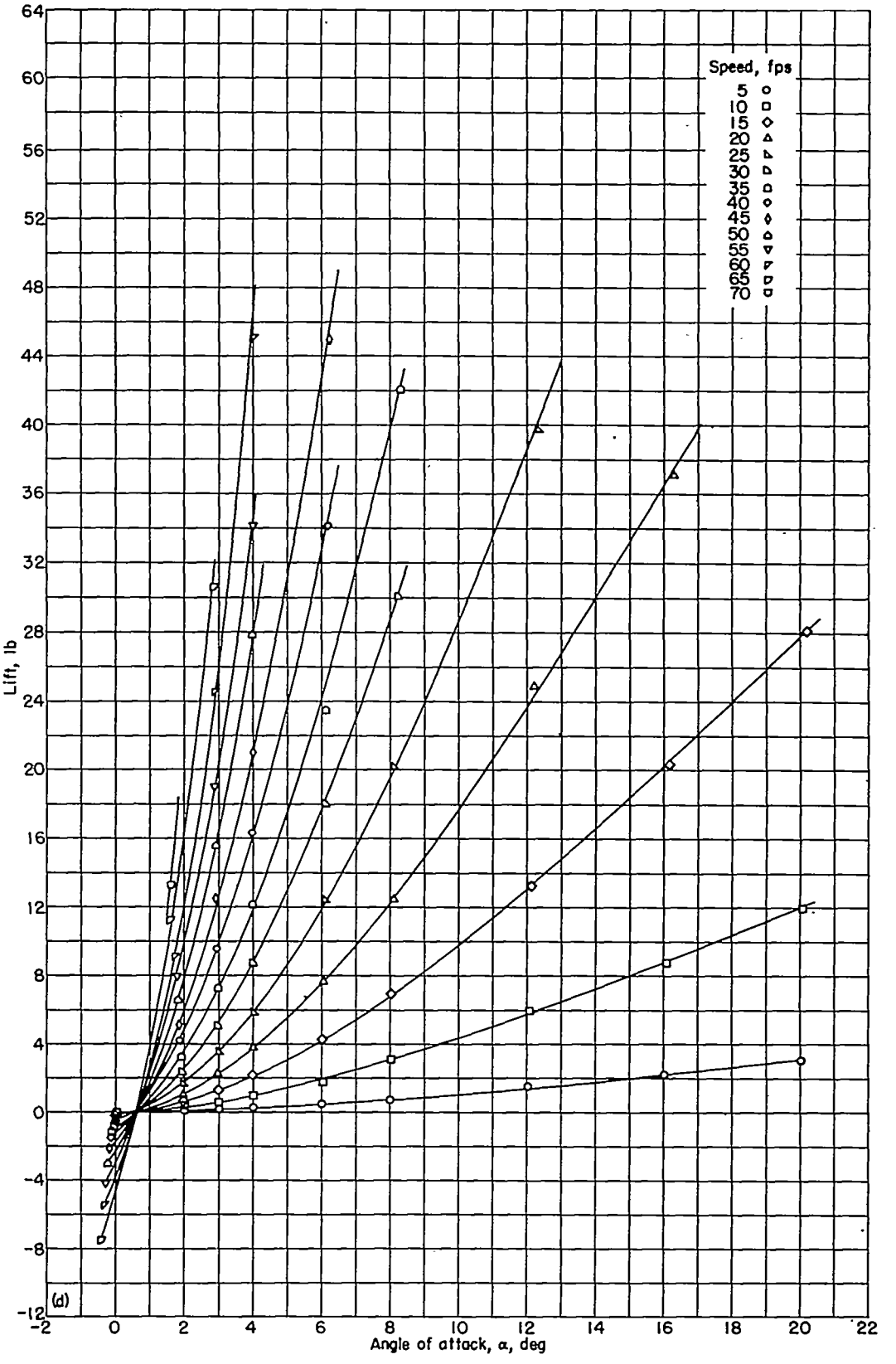

(d) Depth of submersion, 6.0 inches.

FIGURE 8.—Concluded.

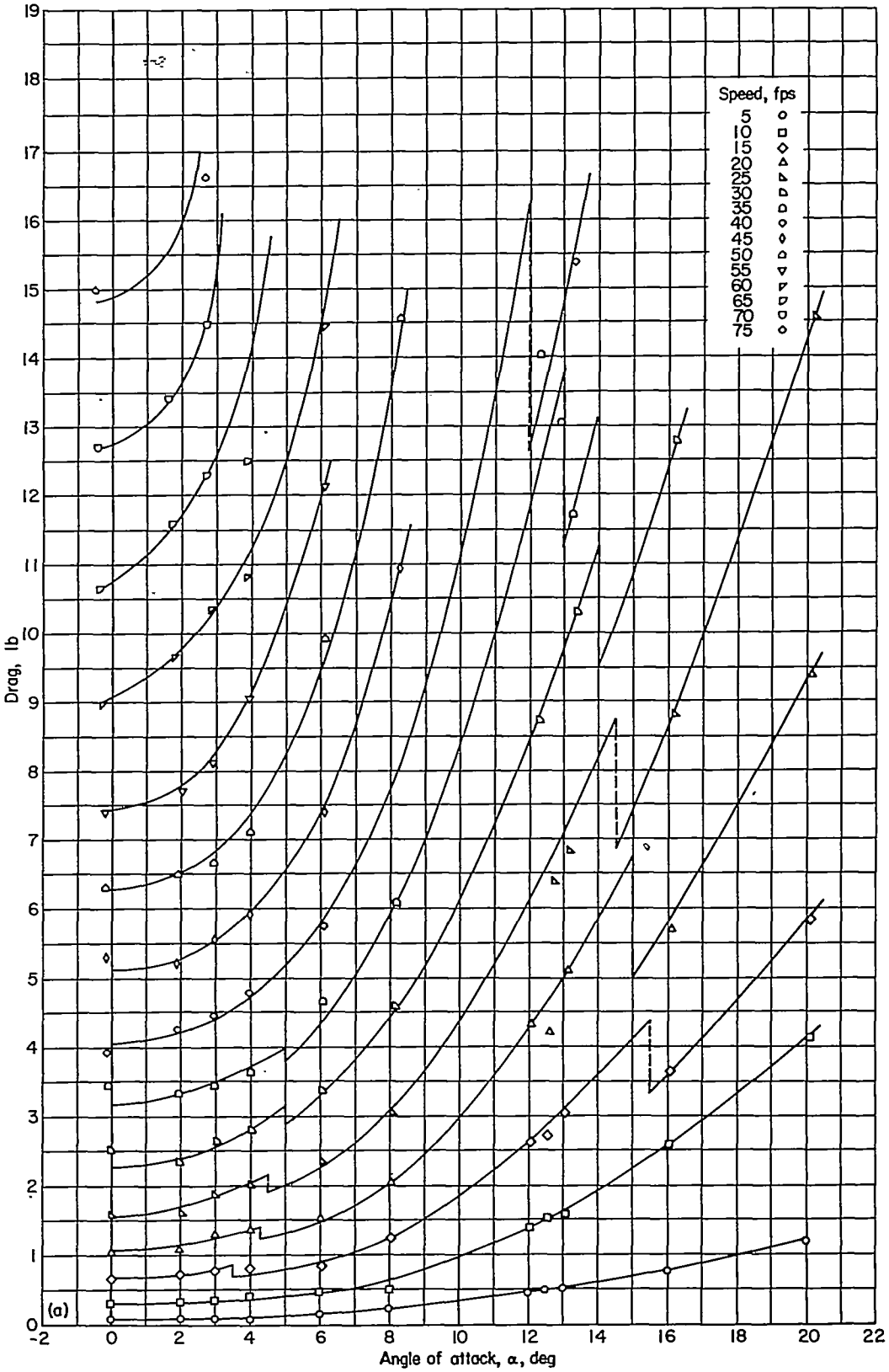

(a) Depth of submersion, 0.5 inch.

FIGURE 9.—Drag on the aspect-ratio-0.125 flat plate. (Dash lines indicate discontinuities associated with flow changes.)

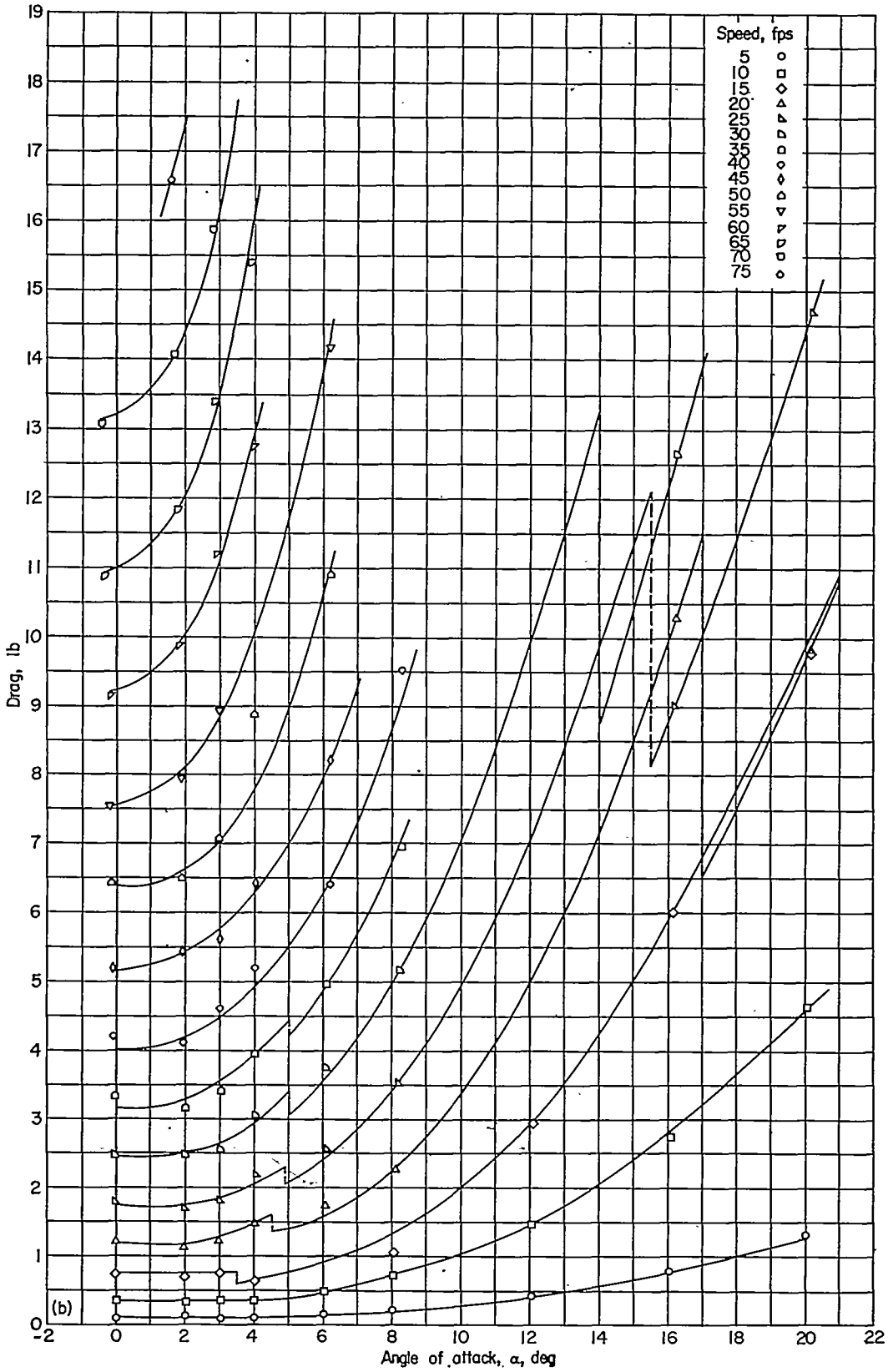

(b) Depth of submersion, 1.0 inch.

FIGURE 9.—Continued.

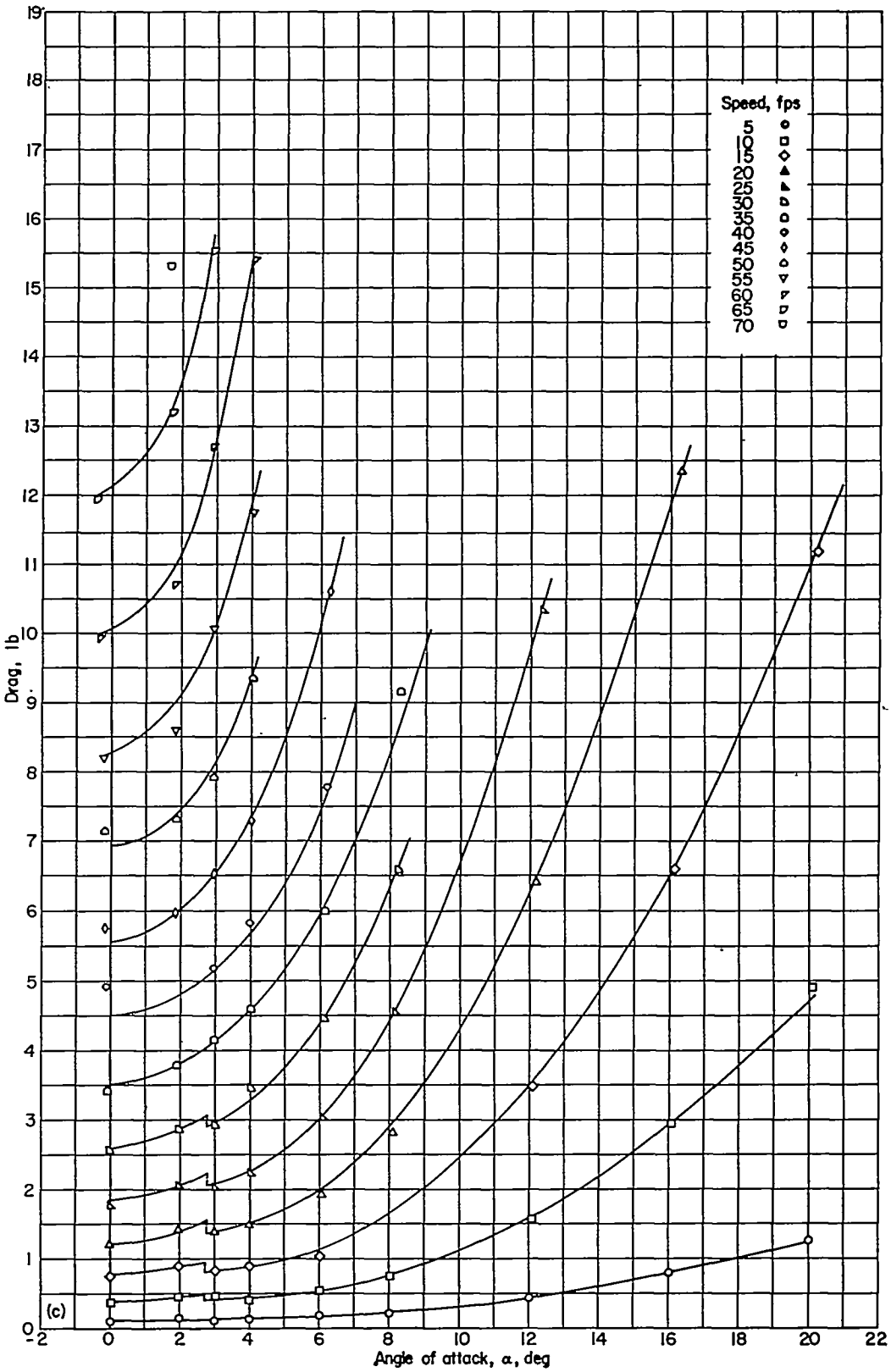

(c) Depth of submersion, 3.0 inches.

FIGURE 9.—Continued.

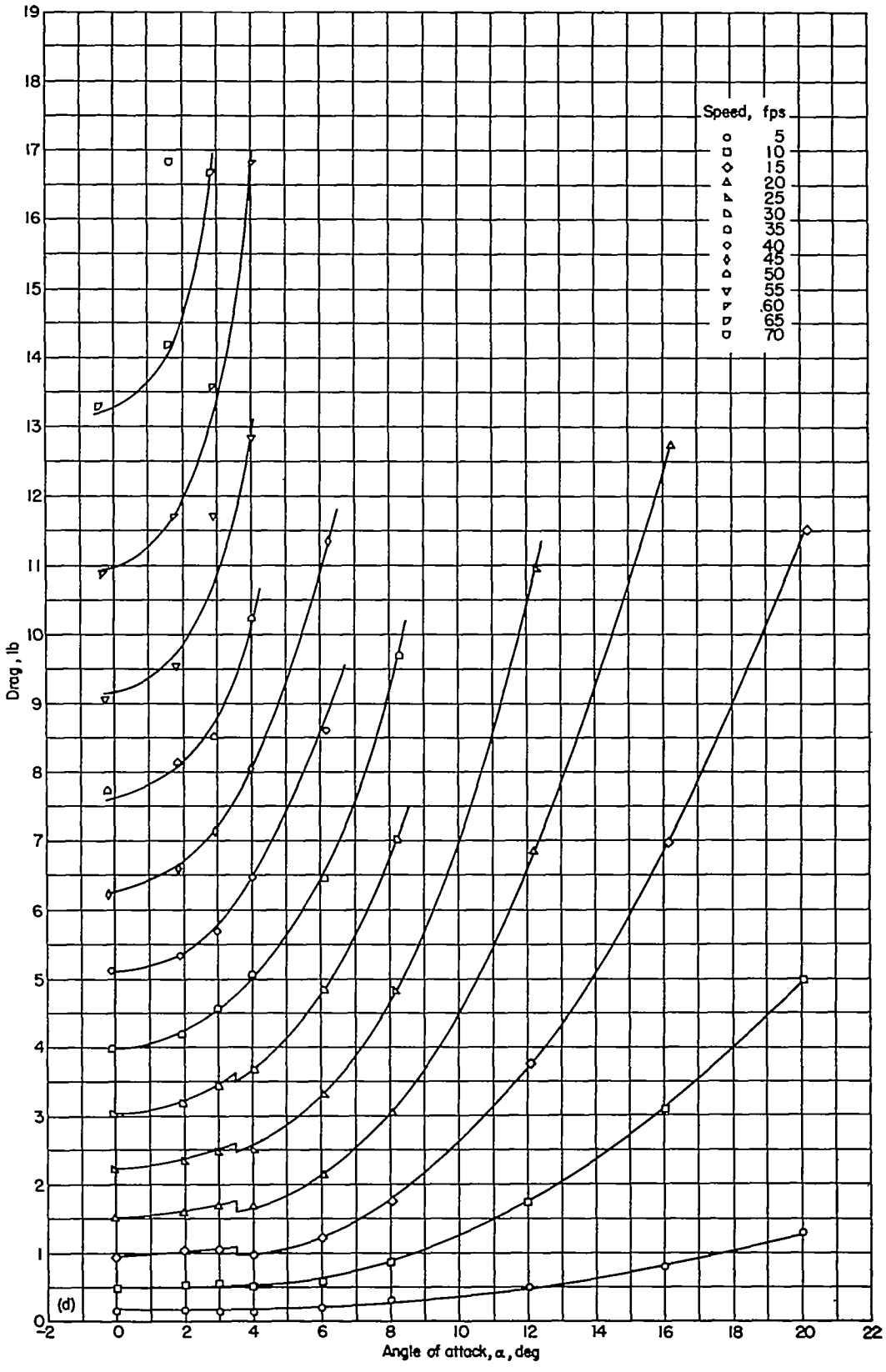

(d) Depth of submersion, 6.0 inches.

FIGURE 9.—Concluded.

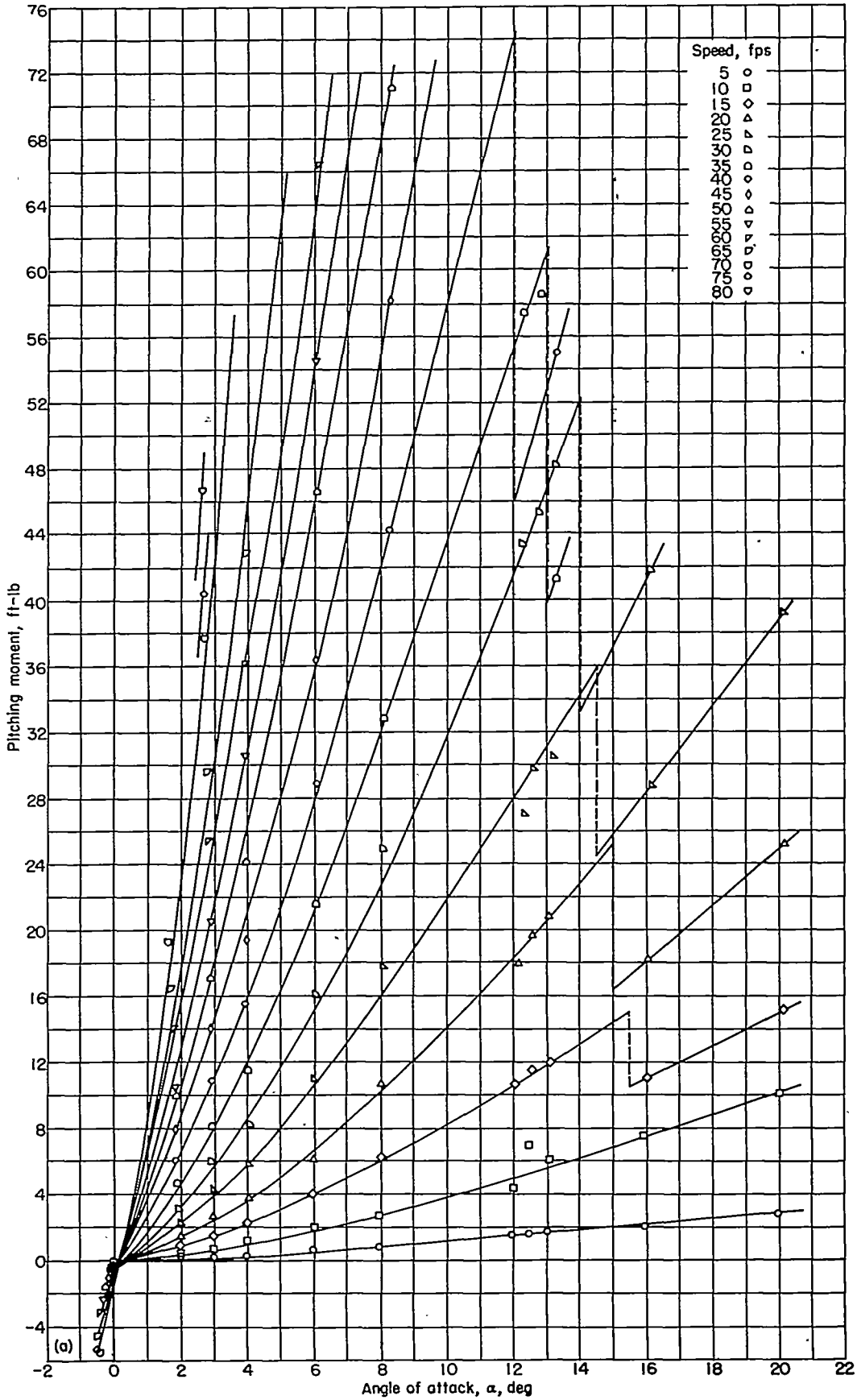

(a) Depth of submersion, 0.5 inch.

FIGURE 10.—Pitching moment on the aspect-ratio-0.125 flat plate. (Dash lines indicate discontinuities associated with flow changes.)

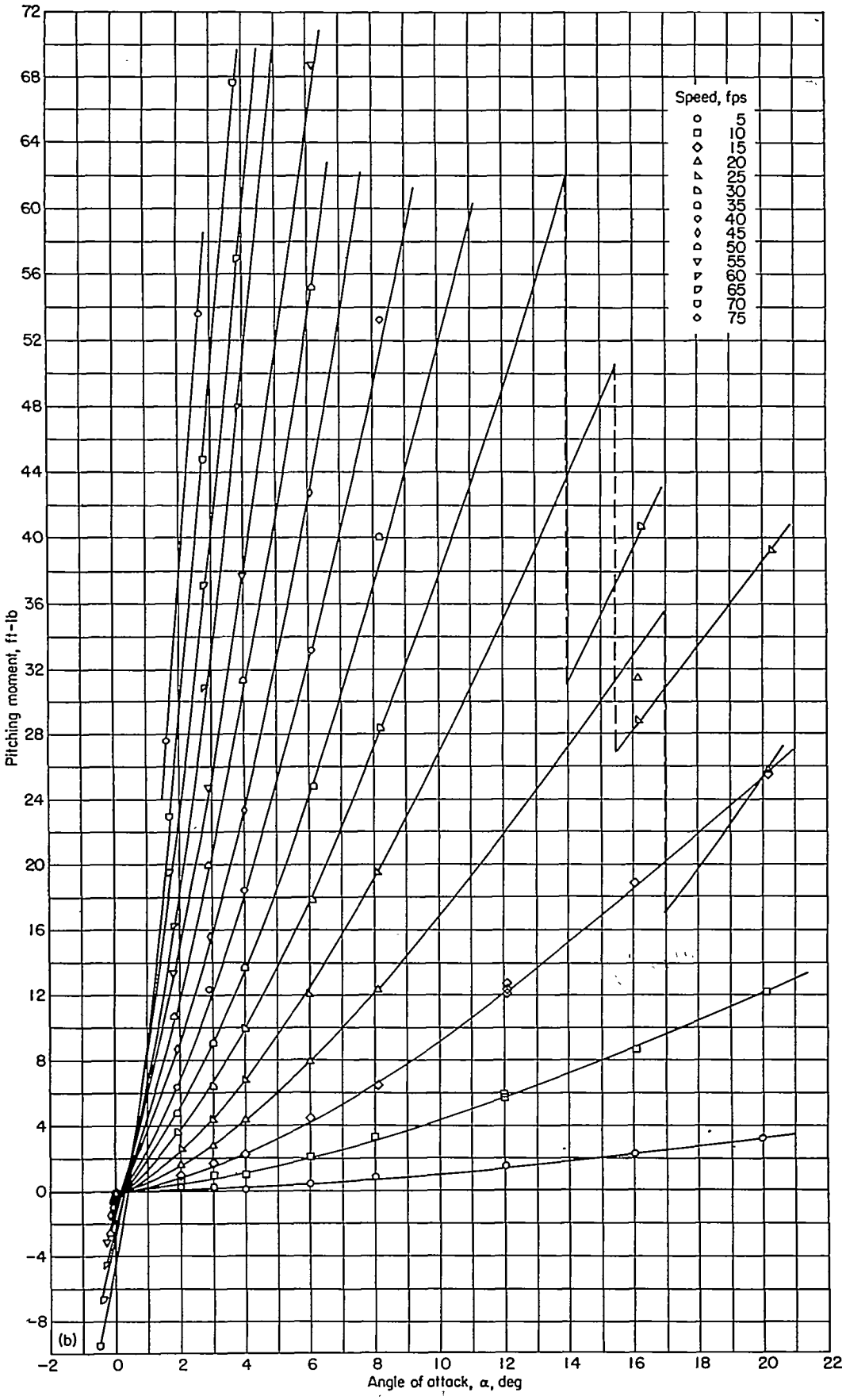

(b) Depth of submersion, 1.0 inch.

FIGURE 10.—Continued.

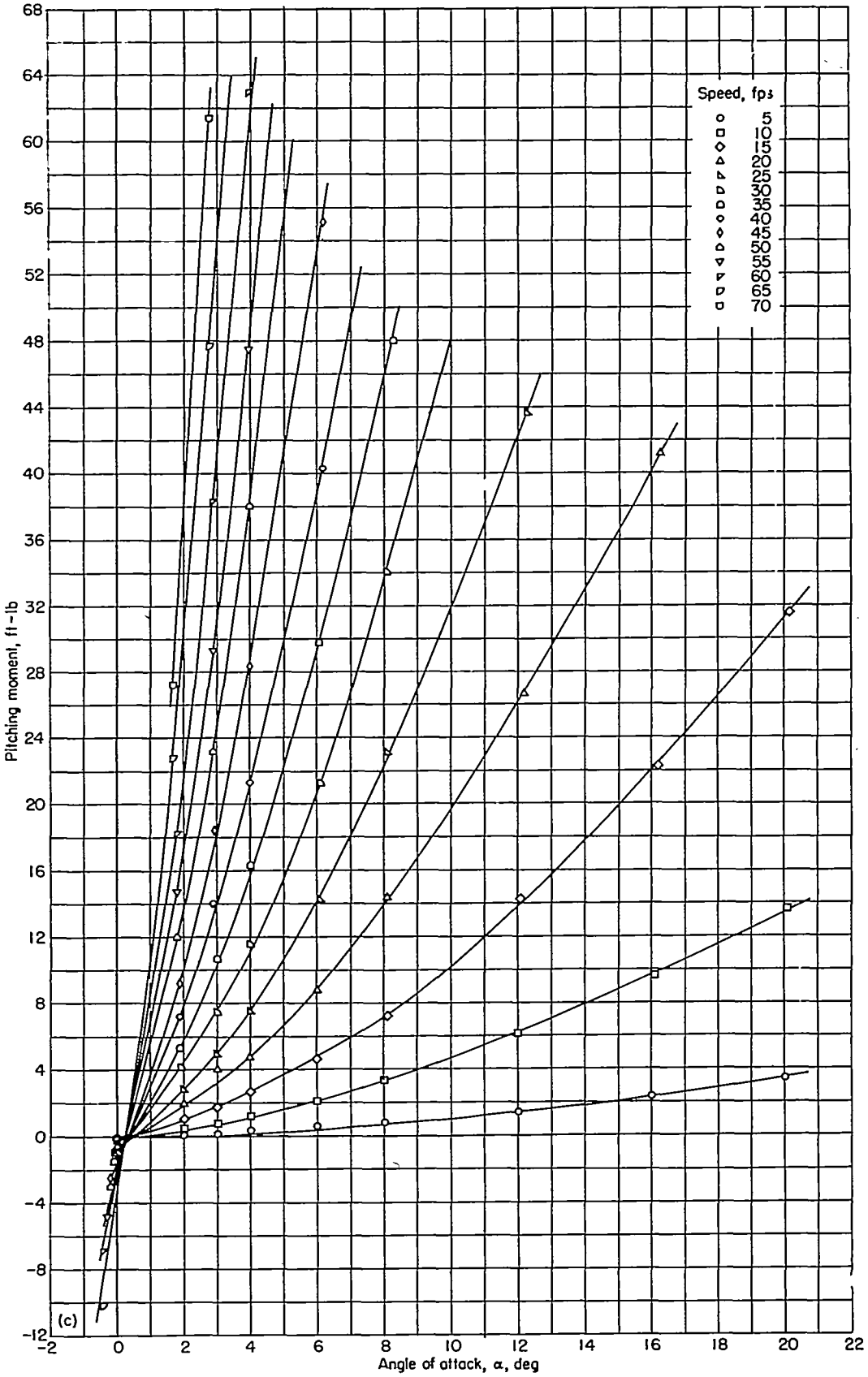

(c) Depth of submersion, 3.0 inches.

FIGURE 10.—Continued.

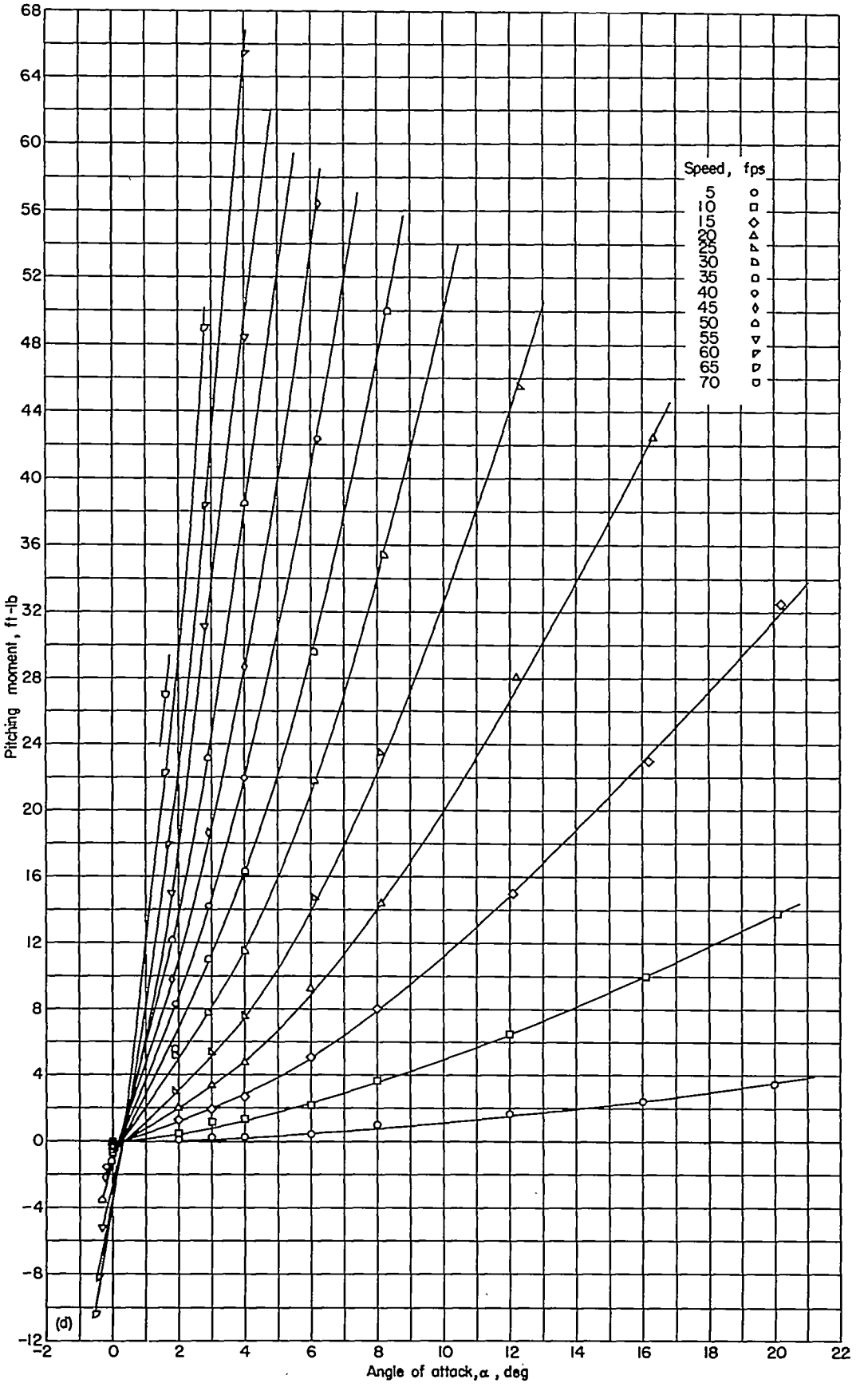

(d) Depth of submersion, 6.0 inches.

FIGURE 10.—Concluded.

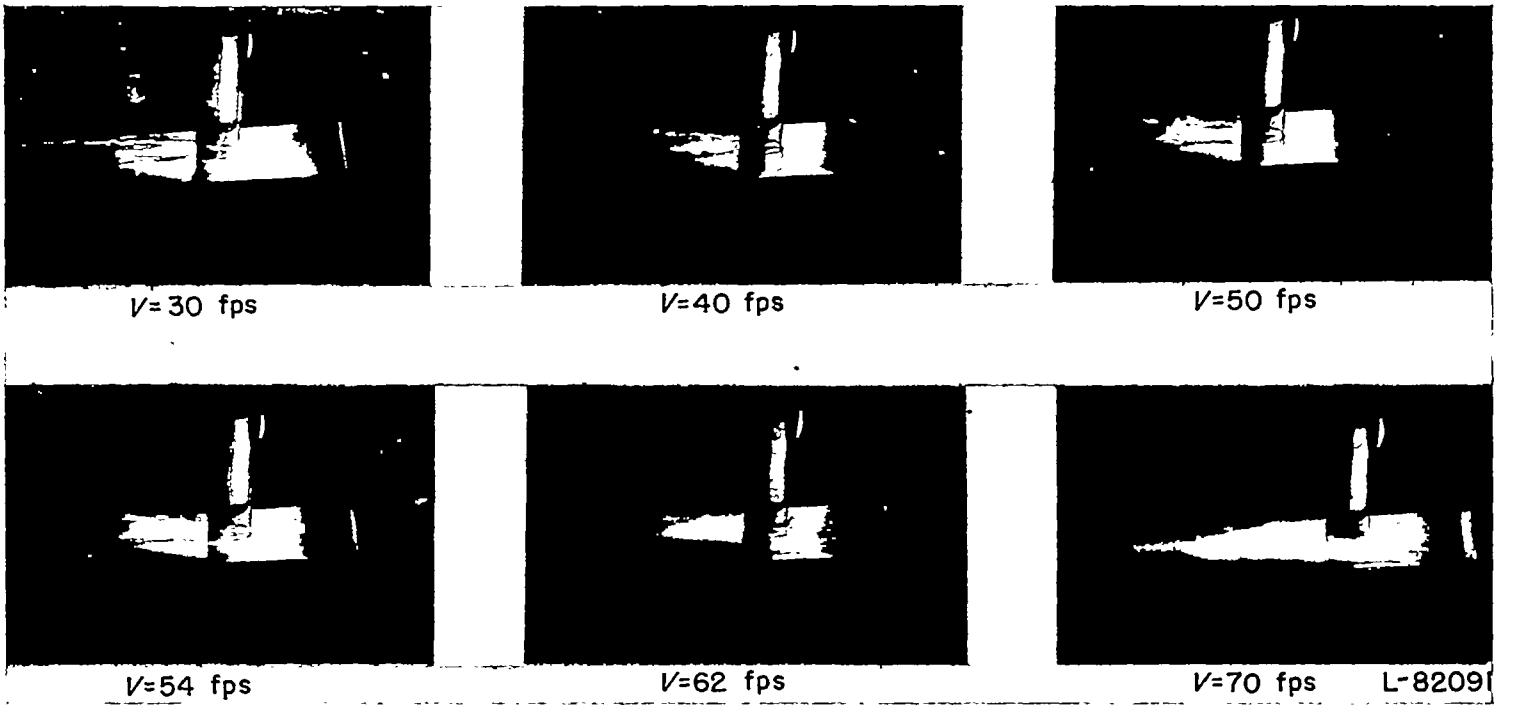

FIGURE 11.—Sequence photographs of a typical run showing the formation of cavitation for the aspect-ratio-0.25 flat plate. (Angle of attack, 2°; depth of submersion, 0.5 inch.)

VISIBLE FLOW CHANGES AND THEIR EFFECTS

Cavitation.—Cavitation at the leading edge occurred at high speeds for all three aspect ratios for all depths. Sequence photographs of a typical run showing the formation of cavitation are presented in figure 11. At a speed of 30 feet per second no cavitation has occurred and the bright area at the leading edge in this instance is merely a reflection caused by the lighting used. Although it cannot readily be seen in this figure, a slight widening of the bright area at 40 feet per second indicated the beginning of cavitation. The bright area is noticeably wider at 54 feet per second; at 62 feet per second, an area becomes evident at the ends of the leading edge where the cavitation is not so strong as in the middle portion of the cavitation region. This result indicates that the low pressure in this area has been relieved somewhat. This area of pressure relief is still more in evidence at 70 feet per second. The area of pressure relief may have existed from the start of the cavitation but was so small as to be unnoticeable before a speed of 62 feet per second was reached.

The angle of attack designated in this figure and in all other sequence photographs to follow is the angle of attack for the model at rest. Since the angle of attack changes with speed because of structural deflections, the photographs do not correspond exactly to a constant angle of attack.

The high speeds necessary for the inception of cavitation were reached only at very low angles of attack; therefore, the results of cavitation are not readily evident in the data plots.

Figure 12 shows a plot of lift coefficient C_L, drag coefficient C_D, and pitching-moment coefficient C_m against speed at the same condition shown in figure 11. The coefficients seemed to be at a fairly constant value when the cavitation started. As the speed increased the cavitation became more severe and caused the lift coefficient to decrease and the drag coefficient to increase. (The fact that the lift coefficient and

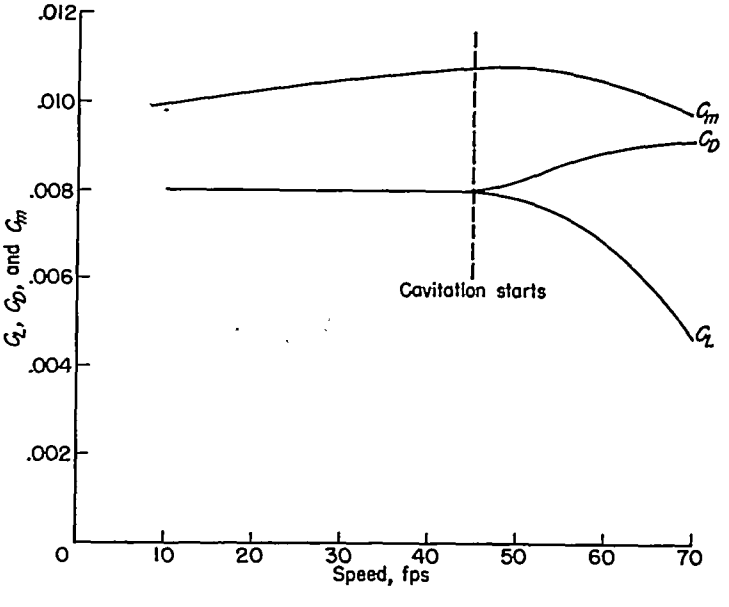

FIGURE 12.—Effect of the formation of cavitation on the force and moment characteristics for the aspect-ratio-0.25 flat plate. (Angle of attack, 2°; depth of submersion, 0.5 inch.)

drag coefficient coincide at speeds before the inception of cavitation is a coincidence peculiar only to the angle of attack illustrated.) The pitching-moment coefficient showed only a slight change with increasing speed after the start of cavitation. The effects of cavitation were similar for all three aspect ratios.

Ventilation.—For all three models at the higher angles of attack and the shallower depths, air was observed to enter the trailing vortices aft of the model. As the speed was increased the entrained air proceeded forward along a helical path inside the vortices until it reached the model when separation took place. The process is shown schematically in figure 13 in which the operation takes the form of a "planing bubble," an air bubble surrounded by a thin film of water in such a manner that no water touches the upper surface of the model.

For the aspect-ratio-1.00 model at a depth of 1 inch, the same process resulted in the formation of "white water," a foamy mixture of air and water which completely covered the upper surface of the model. This effect may be seen in the sequence photographs of figure 14. The helical airstream within the vortices is visible in the photograph taken at 10 feet per second whereas the white water is visible at 12.5 feet per second. When the speed was increased sufficiently, the white water changed to the planing bubble.

The effect of the formation of the white water on the force and moment characteristics is shown in figure 15. The lift coefficient increased until the formation of the white water, after which it decreased slightly and then leveled off. At angles of attack for which no white water formed, the lift coefficient increased up to approximately the speed at which the formation of the white water occurred at the higher angles of attack and then leveled off. Therefore, the principal change in lift coefficient introduced by the formation of the white water is the slight decrease after its formation.

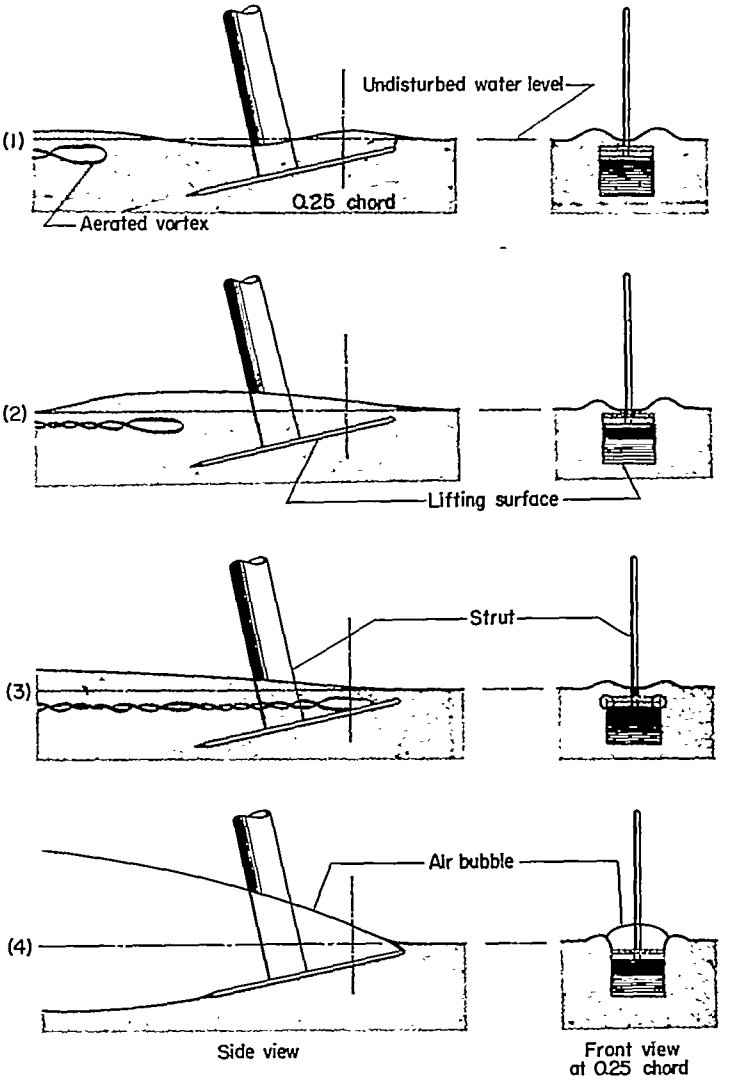

FIGURE 13.—Schematic drawing depicting development of ventilation.

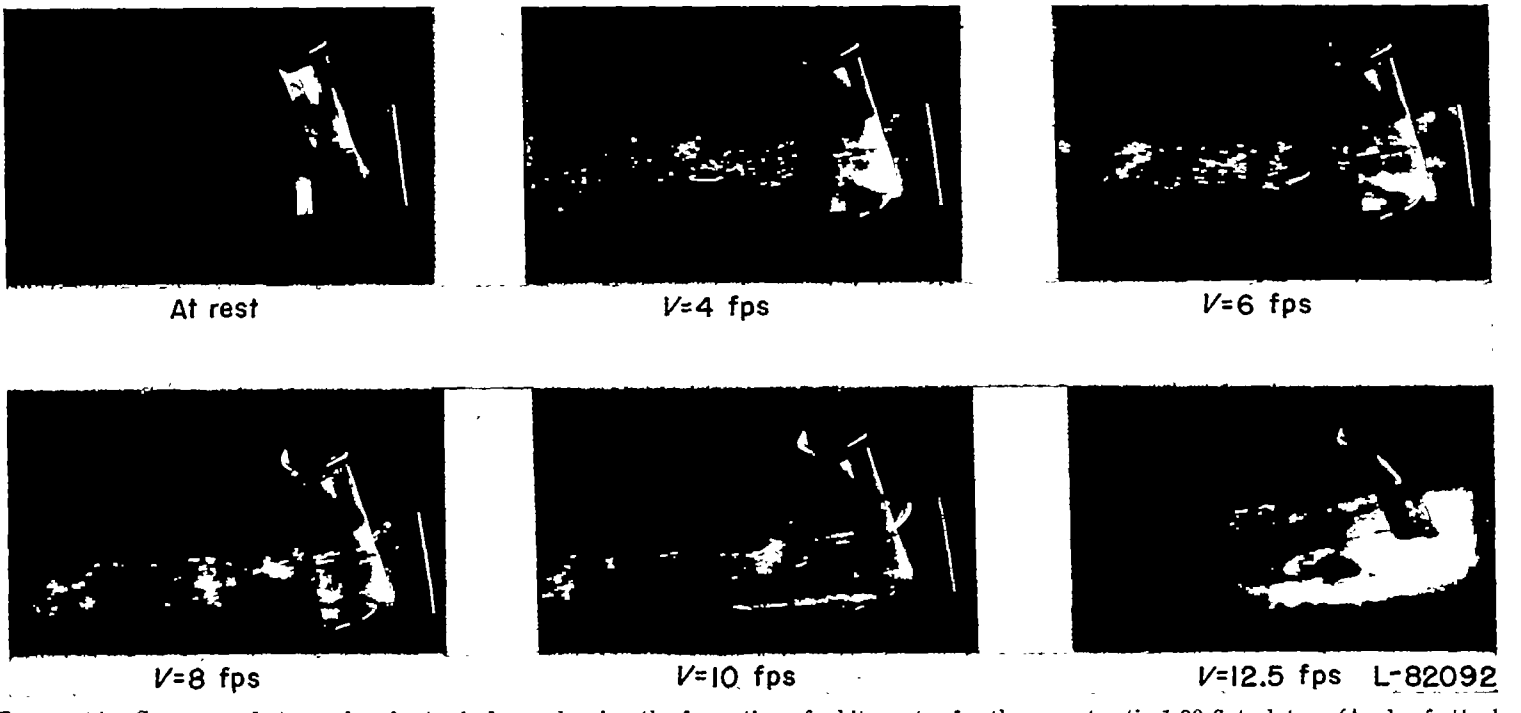

FIGURE 14.—Sequence photographs of a typical run showing the formation of white water for the aspect-ratio-1.00 flat plate. (Angle of attack, 16°; depth of submersion, 1.0 inch.)

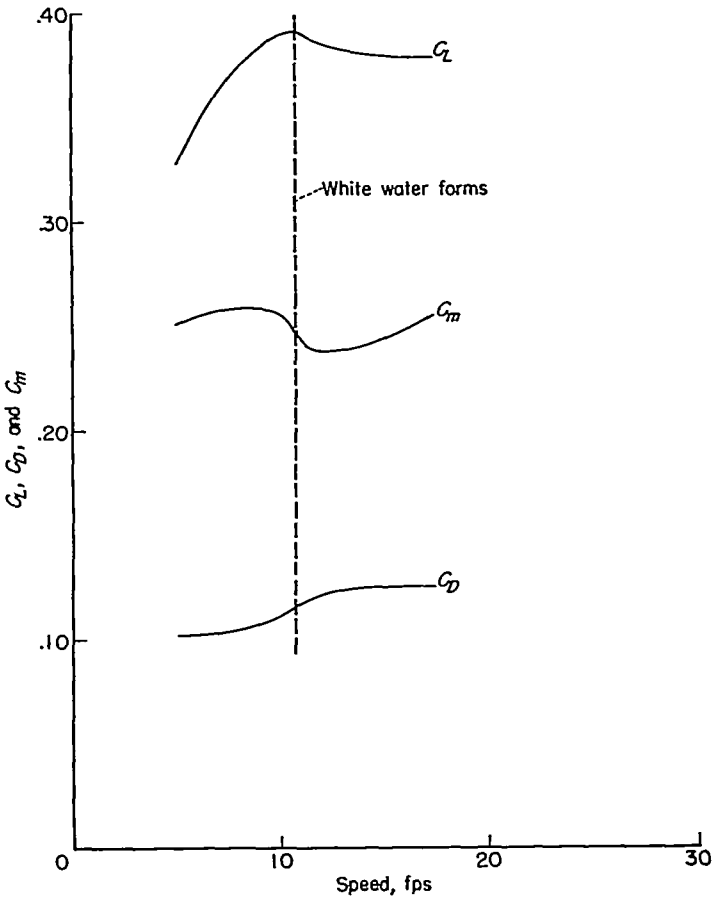

FIGURE 15.—Effect of the formation of white water on the force and moment characteristics of the aspect-ratio-1.00 flat plate. (Angle of attack, 16°; depth of submersion, 1.0 inch.)

The drag coefficient remained more or less constant at the lower speeds, increased with the formation of the white water, and remained constant thereafter. At angles of attack for which no white water occurred, no such drag rise was encountered. The pitching-moment coefficient increased at the lower speeds, decreased sharply with the formation of the white water, and then began to increase again. No sharp decrease was encountered at angles where no white water occurred.

For the aspect-ratio-1.00 model at 0.5-inch depth, the separation took either of the two forms: the white water described previously or the planing bubble which is shown in figure 16. The helical entrained airstreams may be seen advancing within the vortices at speeds of 12 and 13 feet per second whereas at a speed of 15 feet per second the planing bubble has been formed. The model is, in effect, planing under the bubble since no water touches the upper surface. The corresponding force and pitching-moment characteristics are shown in figure 17. All three coefficients increase at the low speeds and then decrease sharply with the formation of the planing bubble, primarily because of the loss of all upper-surface lift. The decrease in lift coefficient is of the order of that to be expected for the transition from the submerged to the planing stage.

The ventilation boundaries for the aspect-ratio-1.00 surface at 0.5-inch depth are presented in figure 18 as a plot of angle of attack against speed. The present tests were run at constant angles of attack while increasing the speed; this procedure corresponds to moving from left to right along horizontal lines in this figure. Below 11.5° no separation was found. Along the line of planing-bubble inception designated A, the planing bubble was the only type of separation encountered. At angles above 12° the line of white-water inception was first encountered but as the speed was further increased the type of separation changed from the white

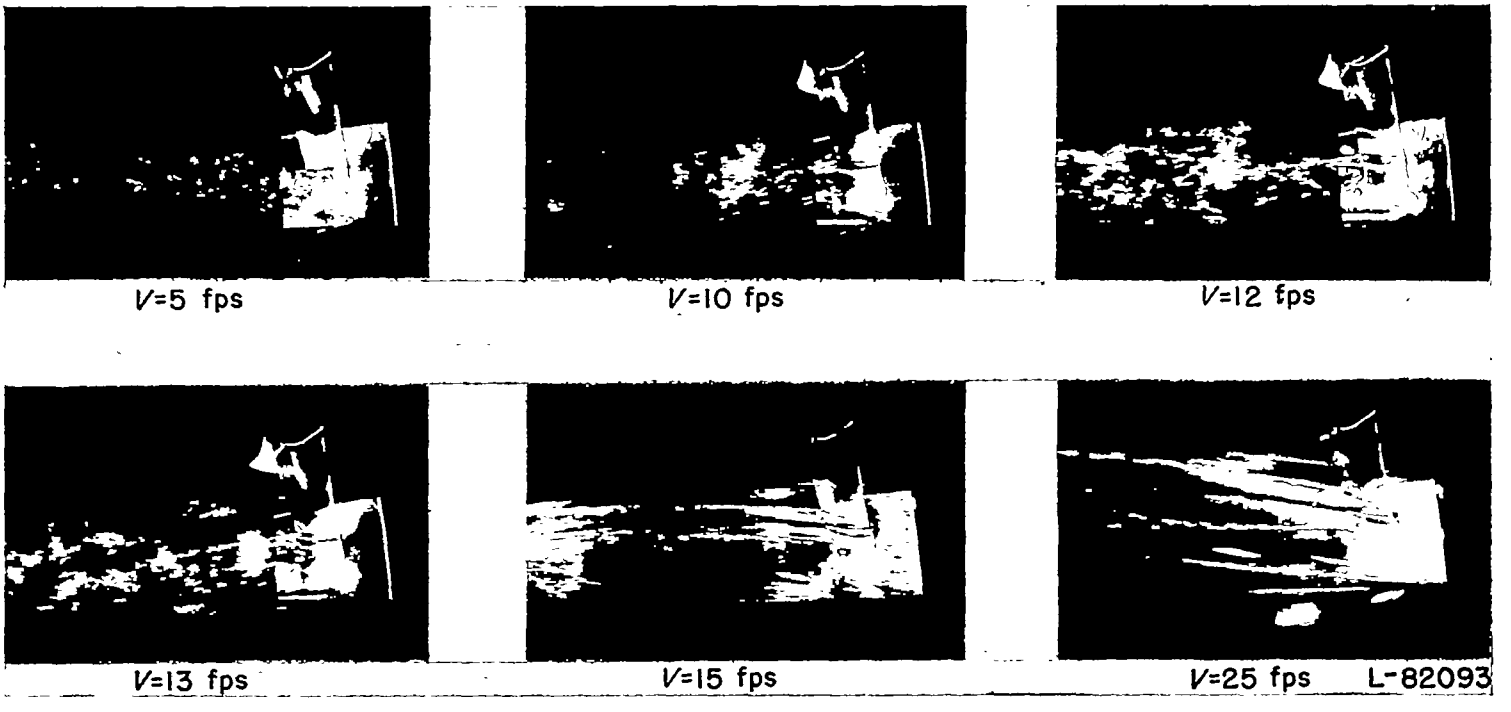

FIGURE 16.—Sequence photographs of a typical run showing the formation of the planing bubble for the aspect-ratio-1.00 flat plate. (Angle of attack, 12°; depth of submersion, 0.5 inch.)

water to the planing bubble as the line of secondary planing-bubble inception designated B was reached. The same type of planing bubble was obtained by crossing either line A or B. The difference in designation was adopted to indicate that in the case of line B the planing bubble was preceded by white water.

The tests indicated that, after the bubble was established, its persistence was very strong. Even in the case of the planing bubble following the white water, there was no tendency for the bubble to collapse or revert to the white water as the speed was decreased almost to standstill. If the speed were held constant and the angle of attack increased, which corresponds to proceeding upward along vertical lines in the figures, white water would occur only at speeds below about 13 feet per second when the white-water inception line was crossed. At speeds above 13 feet per second the planing

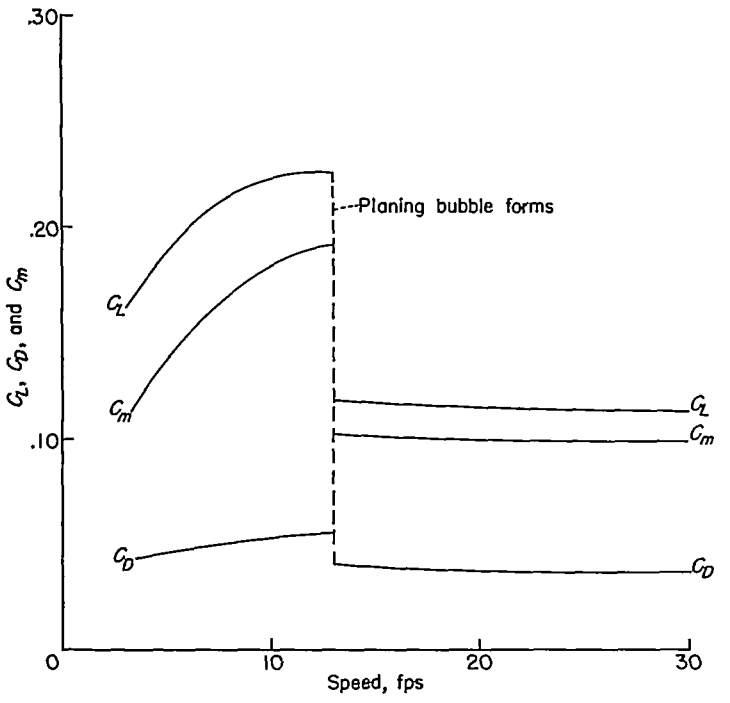

FIGURE 17.—Effect of the formation of the planing bubble on the force and moment characteristics of the aspect-ratio-1.00 flat plate. (Angle of attack, 12°; depth of submersion, 0.5 inch.)

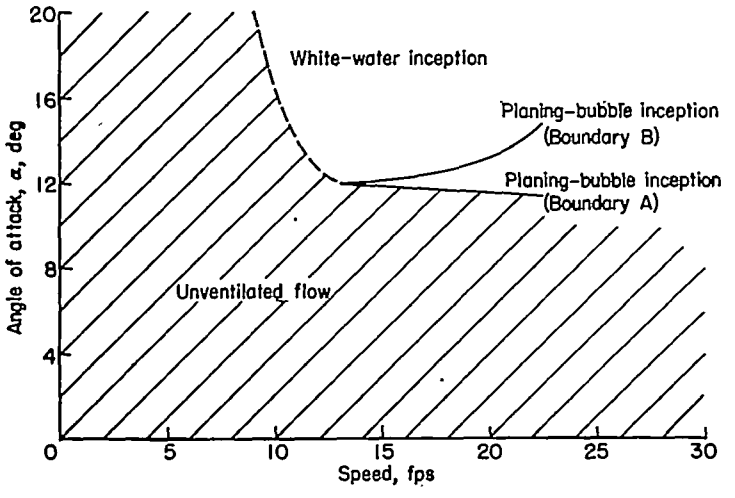

FIGURE 18.—Ventilation boundaries for the aspect-ratio-1.00 plate at a depth of submersion of 0.5 inch.

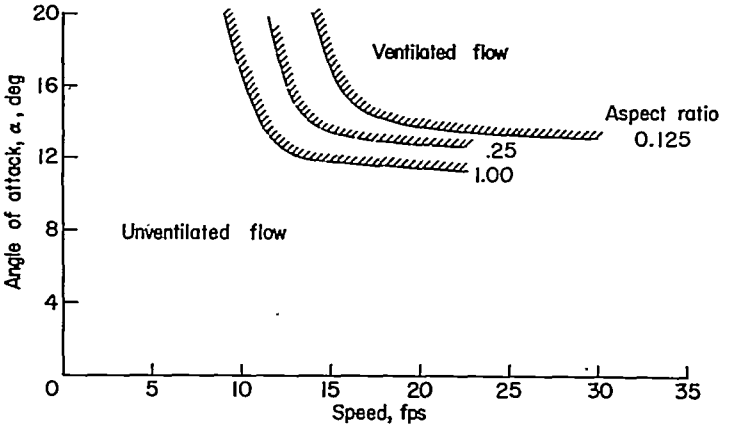

FIGURE 19.—Ventilation boundaries for the low-aspect-ratio flat plates at a depth of 0.5 inch.

bubble would occur as soon as the planing-bubble inception line A was crossed and would not change to white water with further increase in the angle of attack.

For the plates having aspect ratios of 0.25 and 0.125 the coefficients decreased gradually with increasing speed until the ventilation occurred, in contrast to the increase found for the aspect-ratio-1.00 plate. The white-water type of separation which occurred for the aspect-ratio-1.00 plate did not occur for either of the plates having lower aspect ratios for any combination of speed and angle tested. Instead the separation always took the form of a planing bubble with the effects on the characteristics being similar to those described previously for the aspect-ratio-1.00 surface.

The ventilation boundaries for the three surfaces at a depth of 0.5 inch are compared in figure 19. The boundaries are similar in shape but are displaced to higher speeds and higher angles of attack with decreasing aspect ratio.

EFFECTS OF ASPECT RATIO AND DEPTH OF SUBMERSION IN THE REGION OF UNDISTURBED FLOW

The effect of aspect ratio on the lift and drag characteristics at a depth of 6.0 inches is shown in figure 20. At this depth, preliminary computations indicated that the effect of the free surface would be small. The curves of lift coefficient against angle of attack show the nonlinearity common to low-aspect-ratio surfaces. This nonlinearity increased and the lift coefficient for a given angle of attack decreased with decreasing aspect ratio.

The curves of drag coefficient against lift coefficient indicate a slight decrease in drag coefficient for a given lift coefficient with increasing speed (Reynolds number) and a much greater decrease with the increase in aspect ratio. The lift-drag polars for the surfaces having aspect ratios of 1.00 and 0.125 are presented only for a speed of 10 feet per second since the trends with aspect ratio are the same at other speeds. The lift-drag ratios increase with increasing aspect ratio except for the very low lift-coefficient range where the drag discontinuity noted on the data plots apparently has a greater effect for the surfaces having aspect ratios of 0.25 and 0.125; thus, the lift-drag ratios for these surfaces become greater than those for the aspect-ratio-1.00 surface.

The effect of changing the depth of submersion on lift coefficient for the three aspect ratios is shown in figure 21.

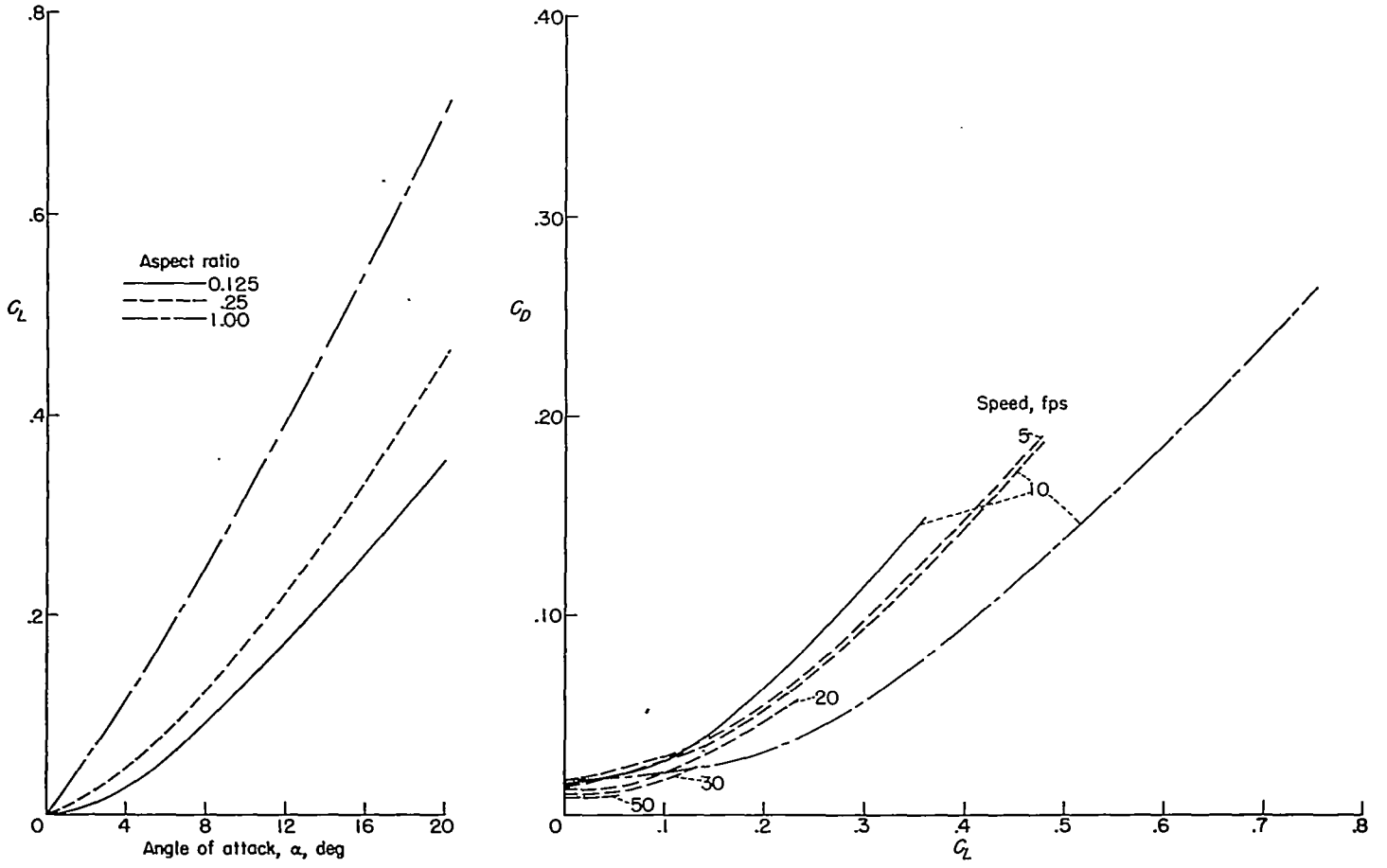

FIGURE 20.—The lift and drag characteristics of the low-aspect-ratio flat plates at a depth of 6.0 inches.

Values of the ratio of the lift coefficient at a given depth to the lift coefficient at a depth of 6 inches C_L/C_{L_6} are plotted against angle of attack with depth of submersion as the parameter in figure 21 (a) and against depth of submersion for an angle of attack of 12° in figure 21 (b). The lift coefficient decreased as the free surface was approached, the decrement in lift coefficient becoming less as the aspect ratio was reduced. The reduction in the decrement of lift coefficient in a change from an aspect ratio of 0.25 to an aspect ratio of 0.125 was considerably greater than that found in a change from an aspect ratio of 1.00 to an aspect ratio of 0.25. The loss in lift was greatest at the lower angles of attack for all three aspect ratios at all depths. The decrement in lift coefficient was considerably reduced as the angle of attack was increased to 12°, at which point it reached a minimum value and changed only slightly with further increase in the angle of attack. A large part of the change at the lower angles of attack may be explained by recalling that the depth of submersion was measured near the leading edge. Thus, as the angle of attack was decreased for a given depth of submersion, the average depth of the plate decreased.

The effect of changing the depth of submersion on the drag coefficient is shown in figure 22 to be similar to the effect on the lift coefficient. Like the lift coefficient, the drag coefficient decreased as the model approached the water surface as would be expected because the induced drag coefficient, which is especially important at these low aspect ratios, is a function of the lift coefficient. The reduction in decrement in drag coefficient in a change from aspect ratio 0.25 to aspect ratio 0.125 was about the same as that obtained in a change from aspect ratio 1.00 to aspect ratio 0.25.

Since the decrease in drag coefficient was less than the decrease in lift coefficient, the lift-drag ratios for all three aspect ratios decreased as the models approached the free water surface. At the depths investigated, the strut drag was small in relation to the total drag. It might be well to point out, however, that, as the depth increases, the strut drag naturally increases also; thus, at some depth, the lift-drag ratio will start to decrease with increasing depth.

The curves of both lift- and drag-coefficient ratios against depth seem to approach the value at a depth of 6.0 inches more or less asymptotically; this fact indicates that at the 6.0-inch depth the surface effect may be considered negligible.

The location of the center of pressure as a function of the angle of attack with depth of submersion as a parameter is shown in figure 23 for all three surfaces. In general, the center of pressure moved forward with decreasing angle of attack and increasing aspect ratio for all three aspect ratios. Changing the angle of attack had a much greater effect at the lower angles of attack, the apparent center of pressure

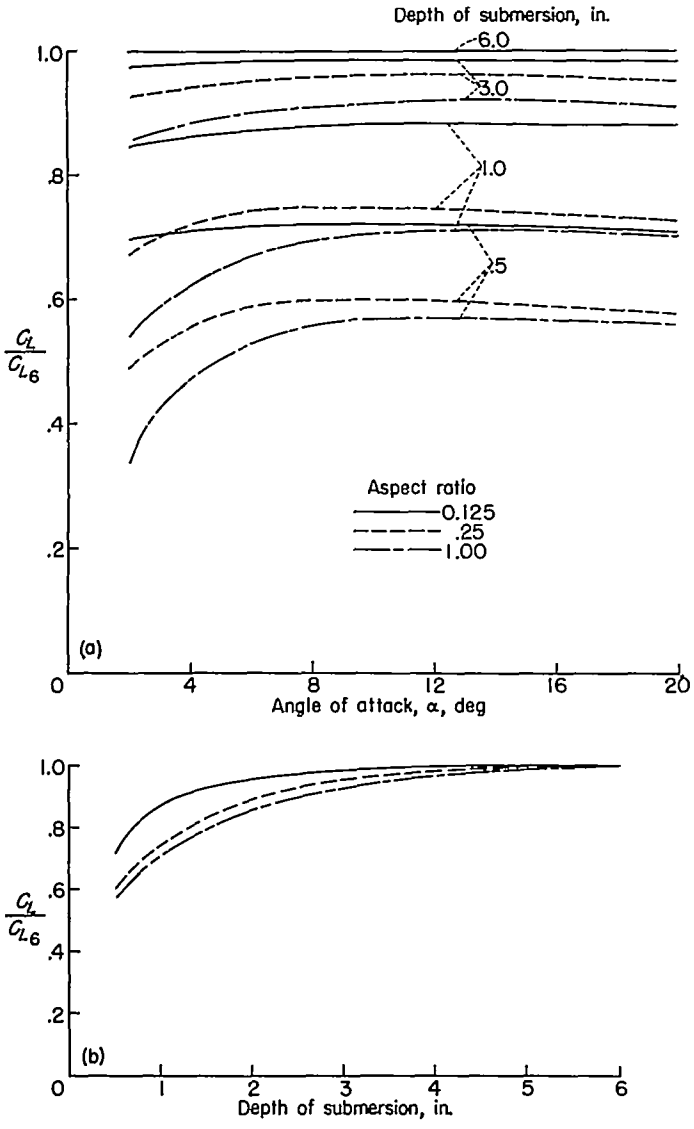

(a) Effect of angle of attack.

(b) Effect of depth of submersion. Angle of attack, 12°.

FIGURE 21.—The variation of the lift characteristics due to changing depth of submersion.

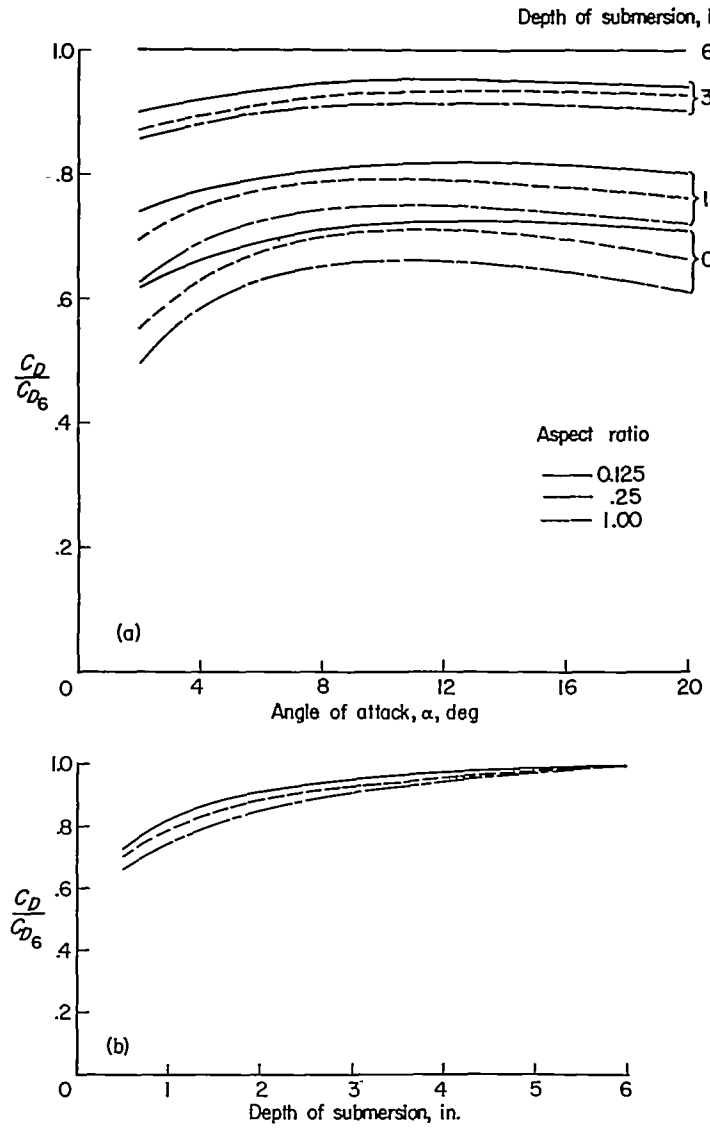

(a) Effect of angle of attack.

(b) Effect of depth of submersion. Angle of attack, 12°.

FIGURE 22.—The variation of the drag characteristics due to changing depth of submersion.

even occurring forward of the leading edge at the lowest angles of attack at 0.5- and 1.0-inch depths. This effect indicates an increase in negative pressure on the upper surface near the leading edge as the water surface is approached or the presence of a suction force over the aft portion of the bottom of the model at low angles of attack or both.

For the surfaces having aspect ratios of 1.00 and 0.25, the center of pressure moved forward with decreasing depth of submersion for all angles of attack. For the aspect-ratio-0.125 model this trend held true only at angles below 8°; above 8°, the center of pressure moved aft with decreasing depth of submersion.

At the higher angles of attack for all three models the center of pressure seems to be approaching a point about ⅝ chord forward of the trailing edge. For the aspect-ratio-1.00 model, rearward movement of the center of pressure occurred at the low angles for depths of 3.0 and 6.0 inches.

THEORY AND COMPARISON WITH EXPERIMENT

GENERAL

A theory was desired which would provide for the determination of the lift at large depths and would be amenable to possible modification by the method of images to account for the effects of the free water surface.

Bollay (ref. 4) and Weinig (ref. 5) have developed aerodynamic theories to apply to low-aspect-ratio surfaces. Flax and Lawrence (ref. 1), in addition to reviewing these and other low-aspect-ratio theories, have presented a semi-empirical approach of their own. These theories, however, do not offer themselves readily to modification by the method of images so an analysis was made to devise a more easily adaptable theory.

The method of Falkner (ref. 6), which is based on linear potential-flow theory, has been found to apply to a wide

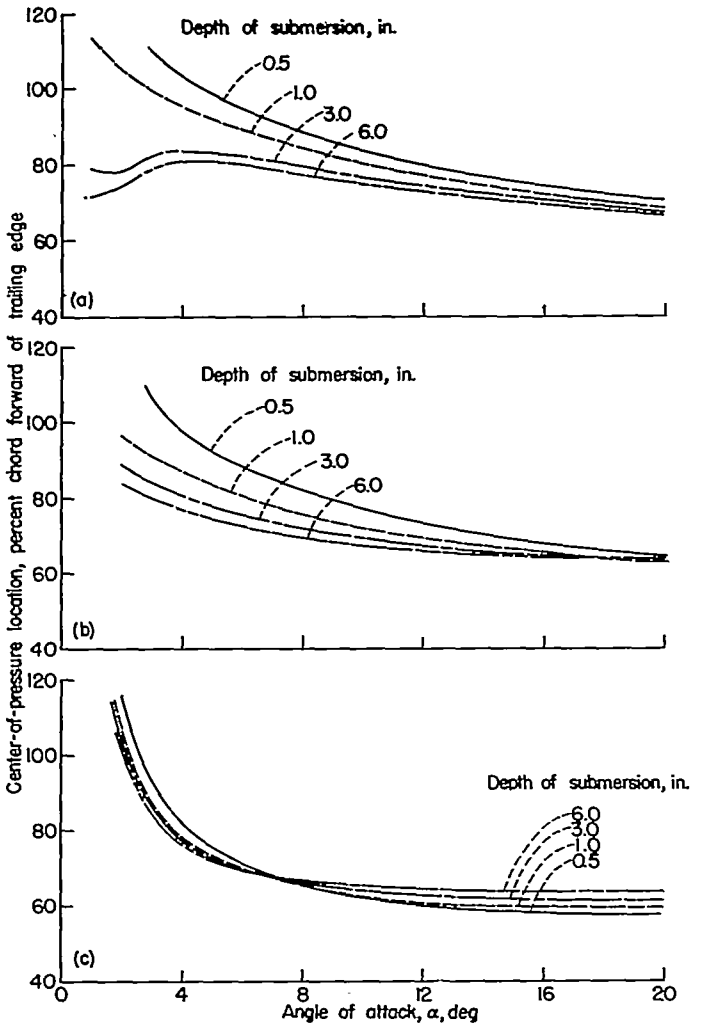

(a) Aspect ratio, 1.00.

(b) Aspect ratio, 0.25.

(c) Aspect ratio, 0.125.

FIGURE 23.—The location of the center of pressure as a function of the angle of attack and the depth of submersion.

range of plan forms at high aspect ratio. The lifting surface in this method is replaced by a system of horseshoe vortices distributed both spanwise and chordwise and the method would lend itself to application of the method of images. Falkner's method was therefore modified to apply to low-aspect-ratio surfaces by introducing nonlinearity and some simplifications were introduced which apply to the present case. This modification is presented in the appendix of this report.

CORRECTIONS TO EXPERIMENTAL DATA

In order to obtain an exact comparison between the data obtained in the present tests and the theories mentioned in the previous section, the tares and interferences would have to be eliminated. Their effect on the lift was expected to be small, however, so that comparisons with the data as obtained were deemed to be valid.

The finite water depth has an effect on the lift coefficient since it imposes a limitation on the speed of wave propagation. Previous experience indicates that the corrections necessary to account for this effect for the low aspect ratios under consideration may be assumed to be negligible. Computations were made to determine the effects of the solid boundaries by using an appropriate array of images. This method is a standard technique used in wind-tunnel work. (For example, see ref. 7.) Because of the small size of the models relative to the tank dimensions, these computations indicate that the effects of the solid boundaries may also be considered negligible.

COMPARISON WITH EXPERIMENT

As pointed out in the previous sections, the free boundary effects of the water surface were negligible at a depth of 6.0 inches. For this reason, a comparison of the lift characteristics at a depth of 6.0 inches from the present test with wind-tunnel data and theoretical results from references 1 to 6 is presented in figure 24. The results of Falkner's linear theory (ref. 6) were obtained by using two vortices spanwise and three vortices chordwise for the half-wing.

The comparison for the aspect-ratio-1.00 surface is presented in figure 24 (a). The present data show excellent agreement with the experimental results of reference 3. The values predicted by the linear theory of Falkner are lower than the data but show reasonable agreement at the low angles. Bollay's theory (ref. 4), on the other hand, predicts values much higher than the data for all angles. The theory of Flax and Lawrence (ref. 1) gives good agreement at the lower angles but gives results which are considerably higher than the data at the higher angles. The theories of Weinig (ref. 5) and the present report show excellent agreement with the data, the theory of the present report being slightly superior at the higher angles. Figure 24 (b) shows the comparison for the aspect-ratio-0.25 surface. The experimental results given in reference 2 are generally lower than those of the present tests but agreement is still reasonable. The predictions of Falkner's linear theory are much lower than the experimental results at all angles but are nevertheless fair approximations for small angles. The theory of Bollay does not seem to have the general characteristics indicated by the data and predicts too high a lift coefficient for most of the range of angles covered. Weinig's method predicts values that are generally lower than the test points whereas the best agreement is provided by the theory of Flax and Lawrence and the method given in the present report. Figure 24 (c) shows the comparison for the aspect-ratio-0.125 surface. Comparable wind-tunnel data for this aspect ratio were not available so that only comparisons with theory are presented. The values predicted by Falkner's linear theory are much lower than the experimental values for all angles of attack and represent only a fair approximation even for the very low angles. The nonlinear theories of Weinig and Flax and Lawrence predict values which are also low when compared with the data but they represent a considerably better approximation than the linear theory. The method given in the present report is in somewhat closer agreement with the data of this investigation except at the very high angles where this method predicts values considerably in excess of those actually achieved. The theory of Bollay (ref. 4) shows excellent agreement over the entire range of angles of attack of these tests.

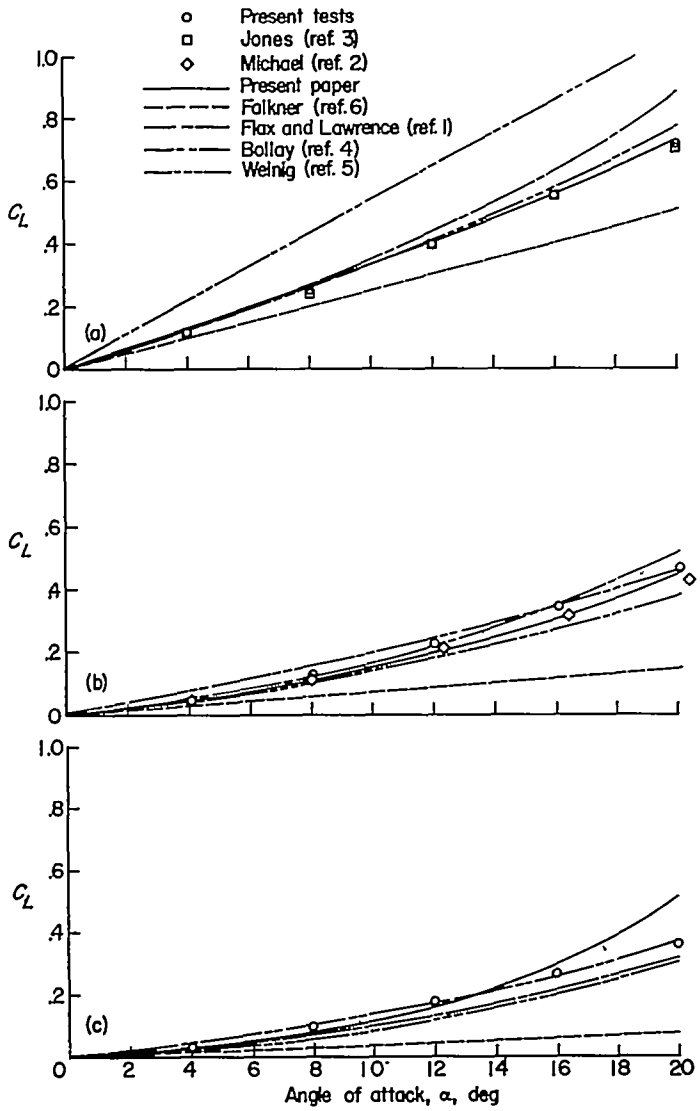

(a) Aspect ratio, 1.00.

(b) Aspect ratio, 0.25.

(c) Aspect ratio, 0.125.

FIGURE 24.—Comparison between experimental and theoretical lift coefficients.

On an overall basis, then, the comparison indicates that the Bollay theory while very accurate for aspect ratio 0.125 departs more and more from the data as the aspect ratio is increased. On the other hand, the linear theory which is inaccurate for all three aspect ratios approaches the data more closely as the aspect ratio is increased. The theories of Flax and Lawrence, Weinig, and the present report show reasonable agreement for all three aspect ratios, the present theory being slightly more accurate on an overall basis. The Flax and Lawrence theory gives only fair agreement at the higher angles of attack for the aspect-ratio-1.00 surface while the Weinig theory gives only fair agreement at the higher angles of attack for the aspect-ratio-0.25 surface and both give only fair agreement for the aspect-ratio-0.125 surface. The present theory gives excellent agreement for aspect ratios of 1.00 and 0.25 for the entire range of angle of attack investigated and reasonable agreement for an aspect ratio of 0.125 up to an angle of attack of 16°. The present theory appears also to offer possibilities of modification to include the effects of proximity of the free water surface by the method of images.

CONCLUSIONS

A simple method has been developed by modification of Falkner's vortex-lattice theory to predict the lift characteristics for unseparated flow at large depths. This method shows good agreement with data from tank tests and wind-tunnel tests for aspect ratios of 1.00 and 0.25 at all angles investigated and for aspect ratio 0.125 at angles below 16°. At angles above 16° for the plate of aspect ratio 0.125, the predicted lift was higher than the experimental lift.

An experimental investigation of the hydrodynamic forces and moments acting on modified rectangular flat plates having aspect ratios of 1.00, 0.25, and 0.125 mounted on a single strut and operating at several depths of submersion indicated that:

Decreasing the aspect ratio for a given angle of attack and depth of submersion decreased the lift coefficient, the drag coefficient, and the lift-drag ratio and caused a rearward movement of the center of pressure.

Decreasing the depth of submersion for a given aspect ratio and angle of attack decreased the lift coefficient, drag coefficient, and lift-drag ratio. The center of pressure moved forward with decreasing depth of submersion for all angles of attack for the plates having aspect ratios of 1.00 and 0.25 and for angles of attack below 8° for the aspect-ratio-0.125 plate. For angles of attack above 8°, the center of pressure for the aspect-ratio-0.125 plate moved aft with decreasing depth of submersion.

Cavitation at the leading edge caused a gradual decrease in lift coefficient, a gradual increase in drag coefficient, and little change in pitching-moment coefficient.

A type of separation at the leading edge at high angles of attack called "white water" and found only for the aspect-ratio-1.00 surface caused a slight decrease in lift coefficient and pitching-moment coefficient and a slight increase in the drag coefficient.

Another type of separation at the leading edge at high angles of attack called the "planing bubble" and found for all three aspect ratios caused a sharp decrease in lift, drag, and pitching-moment coefficients primarily because of loss of upper-surface lift.

The ventilation boundaries defining the start of the separation occurring at high angles of attack moved to higher speeds and higher angles of attack as the aspect ratio was decreased.

LANGLEY AERONAUTICAL LABORATORY,
NATIONAL ADVISORY COMMITTEE FOR AERONAUTICS,
LANGLEY FIELD, VA., *January 19, 1954.*

APPENDIX

MODIFICATION OF FALKNER'S THEORY

The vorticity distribution in the Falkner method is expressed by the double series

$$\gamma=\frac{4bV\tan\alpha}{c}\sqrt{1-\eta^2}\left[\cot\frac{\theta}{2}(a_0+a_1\eta+a_2\eta^2+\ldots)+\sin\theta(b_0+b_1\eta+b_2\eta^2+\ldots)+\sin 2\theta(c_0+c_1\eta+c_2\eta^2+\ldots)+\ldots\right] \quad (1)$$

where

$$\eta=\frac{y}{b/2}$$

$$\cos\theta=\frac{x}{c/2}$$

The variables appearing in equation (1) are defined in figure 25.

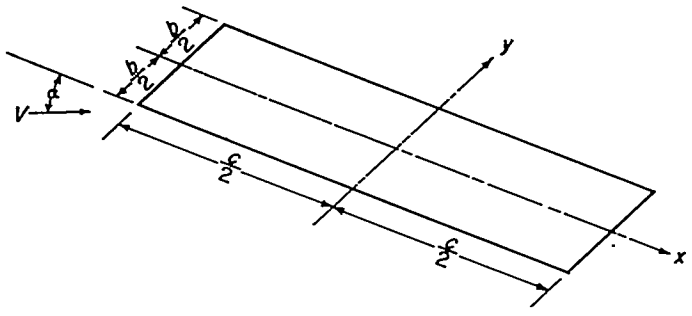

FIGURE 25.—Definitions of variables used in equation (1).

For the symmetrical case such as the present one, the odd powers of η vanish. The circulation is expressed by

$$\Gamma=\int_{-c/2}^{c/2}\gamma\,dx$$

which now becomes

$$\Gamma=\frac{4bV\tan\alpha}{c}\sqrt{1-\eta^2}\left[(a_0+a_2\eta^2+\cdots)\int_{-c/2}^{c/2}\cot\frac{\theta}{2}\,dx+(b_0+b_2\eta^2+\cdots)\int_{-c/2}^{c/2}\sin\theta\,dx+(c_0+c_2\eta^2+\cdots)\int_{-c/2}^{c/2}\sin 2\theta\,dx+\cdots\right] \quad (2)$$

But

$$\frac{x}{c}=\frac{\cos\theta}{2}$$

so that

$$d\left(\frac{x}{c}\right)=-\frac{1}{2}\sin\theta\,d\theta$$

and

$$\cot\frac{\theta}{2}=\frac{1+\cos\theta}{\sin\theta}$$

Therefore,

$$\int_{-c/2}^{c/2}\cot\frac{\theta}{2}\,dx=c\int_{-1/2}^{1/2}\cot\frac{\theta}{2}\,d\left(\frac{x}{c}\right)=-\frac{c}{2}\int_{\pi}^{0}(1+\cos\theta)\,d\theta=\frac{\pi c}{2}$$

Similarly,

$$\int_{-c/2}^{c/2}\sin\theta\,dx=\frac{\pi c}{4}$$

and

$$\int_{-c/2}^{c/2}\sin n\theta\,dx=0$$

where $n>1$. Therefore,

$$\Gamma=4bV\sqrt{1-\eta^2}\tan\alpha\left[\frac{\pi}{2}(a_0+a_2\eta^2+\cdots)+\frac{\pi}{4}(b_0+b_2\eta^2+\cdots)\right] \quad (3)$$

Now,

$$L=\int_{-b/2}^{b/2}\rho V\Gamma\,dy$$

and

$$C_L=\int_{-b/2}^{b/2}\frac{\rho V\Gamma}{\frac{\rho}{2}V^2S}\,dy=\frac{b}{VS}\int_{-1}^{1}\Gamma\,d\eta$$

Hence,

$$C_L=\frac{b}{VS}\int_{-1}^{1}4bV\sqrt{1-\eta^2}\tan\alpha\left[\frac{\pi}{2}(a_0+a_2\eta^2+\cdots)+\frac{\pi}{4}(b_0+b_2\eta^2+\cdots)\right]d\eta$$

$$C_L=\frac{2b^2\pi}{S}\tan\alpha\int_{-1}^{1}\sqrt{1-\eta^2}\left[\left(a_0+\frac{b_0}{2}\right)+\left(a_2+\frac{b_2}{2}\right)\eta^2+\cdots\right]d\eta$$

$$C_L=\frac{b^2\pi^2}{S}\tan\alpha\left[\left(a_0+\frac{b_0}{2}\right)+\frac{1}{4}\left(a_2+\frac{b_2}{2}\right)+\frac{1}{8}\left(a_4+\frac{b_4}{2}\right)+\cdots\right] \quad (4)$$

The evaluation of the unknowns a_n, b_n, and so forth is accomplished as follows:

(1) The vorticity is concentrated into an appropriate number of horseshoe vortices distributed chordwise and spanwise and expressed in terms of equation (1).

(2) At a number of control points, the downwash due to all the vortices as found from the Biot-Savart law is summed.

(3) The downwash angle thus determined at each control point is equated to the local slope of the wing at that control point.

(4) The resulting equations are solved simultaneously for a_n, b_n, and so forth.

The results obtained by the methods used thus far are applicable to any wing shape or aspect ratio by choosing the

proper vortex-lattice distribution. Because of the particular models being considered in the present report, several simplifying assumptions were introduced.

Because of the low aspect ratios under investigation, the assumption is made that the vortices are concentrated so that spanwise only one vortex occurs whose center is at the plane of symmetry. The use of a single vortex means that the terms representing the spanwise distribution may be reduced to one at each chordwise location. This assumption reduces equation (1) to

$$\gamma=\frac{4bV\tan\alpha}{c}\sqrt{1-\eta^2}\left[a_0\cot\frac{\theta}{2}+b_0\sin\theta+c_0\sin 2\theta+\ldots\right] \tag{5}$$

The $\cot\frac{\theta}{2}$ term applies for the straight-line airfoil and the $\sin n\theta$ terms are in effect corrective terms for deviations from the straight line. In order to simplify the equation further, the surfaces are assumed to be represented by the $\cot\frac{\theta}{2}$ term only; this assumption means that the surfaces are now represented by one horseshoe vortex. The final equation for the vorticity therefore is

$$\gamma=\frac{4bV\tan\alpha}{c}\sqrt{1-\eta^2}\,a_0\cot\frac{\theta}{2} \tag{6}$$

In a manner similar to that used in obtaining equation (3), the circulation is obtained as

$$\Gamma=\frac{4bV\tan\alpha}{c}\sqrt{1-\eta^2}\,a_0\frac{\pi c}{2}$$

or

$$\Gamma=2\pi bVa_0\sqrt{1-\eta^2}\tan\alpha \tag{7}$$

According to Glauert (ref. 8), the downwash produced by a simple horseshoe vortex may be expressed by

$$w=\frac{\Gamma}{4\pi}F \tag{8}$$

where F is a position factor which is governed by the relative location of the horseshoe vortex and the point at which the downwash is computed. Combining equation (7) and (8) and setting $\eta=0$, since the vortex is centered at the plane of symmetry, gives

$$\frac{w}{V}=\frac{a_0bF\tan\alpha}{2} \tag{9}$$

Equating this relation to the local slope of the plate, which is $\tan\alpha$, yields

$$a_0=\frac{2}{bF}$$

or in nondimensional form

$$a_0=\frac{2}{F_cA} \tag{10}$$

where

$$F_c=Fc$$

and

$$A=\frac{b}{c}$$

By applying the methods used in obtaining equation (4), the following equation results:

$$C_L=\frac{b}{VS}\int_{-1}^{1}\Gamma\,d\eta$$

Substituting equation (7) into this equation yields

$$C_L=\frac{2\pi b^2}{S}a_0\tan\alpha\int_{-1}^{1}\sqrt{1-\eta^2}\,d\eta$$

or

$$C_L=\frac{2\pi^2b^2}{2S}a_0\tan\alpha \tag{11}$$

Substituting equation (10) into equation (11) and using the relation $S=bc$ yields

$$C_L=\frac{2\pi^2\tan\alpha}{F_c} \tag{12}$$

Thus, the only unknown necessary to determine the lift coefficient as a function of the angle of attack is the position factor F_c.

From reference 8, F is given as

$$F=\frac{x'}{(x')^2+(z')^2}\left[\frac{y'+\frac{b}{2}}{\sqrt{(x')^2+(z')^2+\left(y'+\frac{b}{2}\right)^2}}-\frac{y'-\frac{b}{2}}{\sqrt{(x')^2+(z')^2+\left(y'-\frac{b}{2}\right)^2}}\right]-$$
$$\frac{y'-\frac{b}{2}}{(z')^2+\left(y'-\frac{b}{2}\right)^2}\left[1+\frac{x'}{\sqrt{(x')^2+(z')^2+\left(y'-\frac{b}{2}\right)^2}}\right]+\frac{y'+\frac{b}{2}}{(z')^2+\left(y'+\frac{b}{2}\right)^2}\left[1+\frac{x'}{\sqrt{(x')^2+(z')^2+\left(y'+\frac{b}{2}\right)^2}}\right] \tag{13}$$

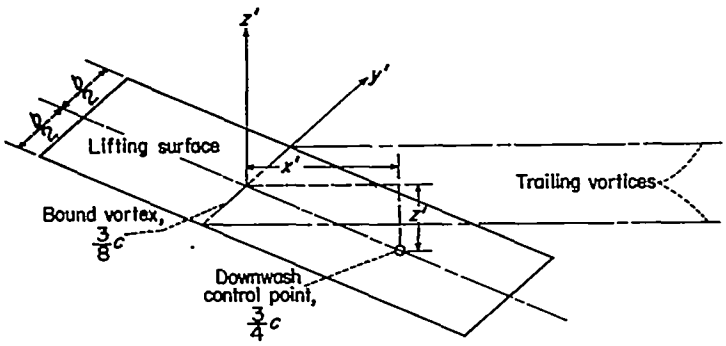

FIGURE 26.—Definitions of variables used in equation (13).

where the variables are defined in figure 26.

From the assumptions made previously, $y'=0$. The single horseshoe vortex is considered to operate at the ⅜-chord point (which is the center of pressure at high angles for all three surfaces tested) and the downwash is summed at the ¾-chord point. The nonlinearity is now introduced by considering the displacements produced by changing the angle of attack.

Substituting

$$x'=\frac{3c}{8}\cos\alpha$$

$$y'=0$$

$$z'=\frac{3c}{8}\sin\alpha$$

into equation (13) yields

$$F=\frac{\cos\alpha}{\frac{3c}{8}}\left[\frac{b}{\sqrt{\left(\frac{3c}{8}\right)^2+\frac{b^2}{4}}}\right]+\frac{b}{\left(\frac{3c}{8}\right)^2\sin^2\alpha+\frac{b^2}{4}}\left[1+\frac{\frac{3c}{8}\cos\alpha}{\sqrt{\left(\frac{3c}{8}\right)^2+\frac{b^2}{4}}}\right] \tag{14}$$

Expressing all measurements in chords and using the fact that $A=\frac{b}{c}$ gives

$$F_c=\frac{8A\cos\alpha}{3\sqrt{\left(\frac{3}{8}\right)^2+\frac{A^2}{4}}}+\frac{A}{\left(\frac{3}{8}\sin\alpha\right)^2+\frac{A^2}{4}}\left[1+\frac{\frac{3}{8}\cos\alpha}{\sqrt{\left(\frac{3}{8}\right)^2+\frac{A^2}{4}}}\right]$$

Clearing of fractions gives

$$F_c=\frac{64A\cos\alpha}{3\sqrt{9+16A^2}}+\frac{64A}{9\sin^2\alpha+16A^2}\left(1+\frac{3\cos\alpha}{\sqrt{9+16A^2}}\right) \tag{15}$$

Solving equation (15) and entering the value of F_c for any particular case into equation (12) now enables the determination of the lift coefficient. These expressions are used in making the computations, the results of which are shown in figure 24.

REFERENCES

1. Flax, A. H., and Lawrence, H. R.: The Aerodynamics of Low-Aspect-Ratio Wings and Wing-Body Combinations. Rep. No. CAL-37, Cornell Aero. Lab., Inc., Sept. 1951.
2. Michael, William H., Jr.: Flow Studies in the Vicinity of a Modified Flat-Plate Rectangular Wing of Aspect Ratio 0.25. NACA TN 2790, 1952.
3. Jones, George W., Jr.: Investigation of the Effects of Variations in the Reynolds Number Between 0.4×10^6 and 3.0×10^6 on the Low-Speed Aerodynamic Characteristics of Three Low-Aspect-Ratio Symmetrical Wings With Rectangular Plan Forms. NACA RM L52G18, 1952.
4. Bollay, William: A Non-Linear Wing Theory and Its Application to Rectangular Wings of Small Aspect Ratio. Z.f.a.M.M., Bd. 19, Nr. 1, Feb. 1939, pp. 21–35.
5. Weinig, F.: Lift and Drag of Wings With Small Span. NACA TM 1151, 1947.
6. Falkner, V. M.: The Calculation of Aerodynamic Loading on Surfaces of Any Shape. R. & M. No. 1910, British A.R.C., 1943.
7. Theodorsen, Theodore: The Theory of Wind-Tunnel Wall Interference. NACA Rep. 410, 1931.
8. Glauert, H.: The Elements of Aerofoil and Airscrew Theory. Cambridge Univ. Press, 1926, p. 158.